You might find this additional information useful...

This article cites 179 articles, 55 of which you can access free at:
http://jn.physiology.org/cgi/content/full/103/1/297#BIBL

This article has been cited by 1 other HighWire hosted article:

Toward discovery science of human brain function
B. B. Biswal, M. Mennes, X.-N. Zuo, S. Gohel, C. Kelly, S. M. Smith, C. F. Beckmann, J. S. Adelstein, R. L. Buckner, S. Colcombe, A.-M. Dogonowski, M. Ernst, D. Fair, M. Hampson, M. J. Hoptman, J. S. Hyde, V. J. Kiviniemi, R. Kotter, S.-J. Li, C.-P. Lin, M. J. Lowe, C. Mackay, D. J. Madden, K. H. Madsen, D. S. Margulies, H. S. Mayberg, K. McMahon, C. S. Monk, S. H. Mostofsky, B. J. Nagel, J. J. Pekar, S. J. Peltier, S. E. Petersen, V. Riedl, S. A. R. B. Rombouts, B. Rypma, B. L. Schlaggar, S. Schmidt, R. D. Seidler, G. J. Siegle, C. Sorg, G.-J. Teng, J. Veijola, A. Villringer, M. Walter, L. Wang, X.-C. Weng, S. Whitfield-Gabrieli, P. Williamson, C. Windischberger, Y.-F. Zang, H.-Y. Zhang, F. X. Castellanos and M. P. Milham
PNAS, March 9, 2010; 107 (10): 4734-4739.
[Abstract] [Full Text] [PDF]

Updated information and services including high-resolution figures, can be found at:
http://jn.physiology.org/cgi/content/full/103/1/297

Additional material and information about *Journal of Neurophysiology* can be found at:
http://www.the-aps.org/publications/jn

This information is current as of May 17, 2010 .

Intrinsic Functional Connectivity As a Tool For Human Connectomics: Theory, Properties, and Optimization

Koene R. A. Van Dijk,[1,2,3] **Trey Hedden,**[1,2] **Archana Venkataraman,**[4] **Karleyton C. Evans,**[5] **Sara W. Lazar,**[5] **and Randy L. Buckner**[1,2,5,6]

[1]*Department of Psychology, Center for Brain Science, Harvard University, Cambridge, Massachusetts;* [2]*Athinoula A. Martinos Center for Biomedical Imaging, Department of Radiology and* [5]*Department of Psychiatry, Massachusetts General Hospital, Charlestown, Massachusetts;* [3]*Department of Neuropsychology and Psychopharmacology, Faculty of Psychology, Maastricht University, Netherlands;* [4]*Computer Science and Artificial Intelligence Laboratory (CSAIL), Massachusetts Institute of Technology, Cambridge, Massachusetts; and* [6]*Howard Hughes Medical Institute, Cambridge, Massachusetts*

Van Dijk KR, Hedden T, Venkataraman A, Evans KC, Lazar SW, Buckner RL. Intrinsic functional connectivity as a tool for human connectomics: theory, properties, and optimization. *J Neurophysiol* 103: 297–321, 2010. First published November 4, 2009; doi:10.1152/jn.00783.2009. Resting state functional connectivity MRI (fcMRI) is widely used to investigate brain networks that exhibit correlated fluctuations. While fcMRI does not provide direct measurement of anatomic connectivity, accumulating evidence suggests it is sufficiently constrained by anatomy to allow the architecture of distinct brain systems to be characterized. fcMRI is particularly useful for characterizing large-scale systems that span distributed areas (e.g., polysynaptic cortical pathways, cerebro-cerebellar circuits, cortical-thalamic circuits) and has complementary strengths when contrasted with the other major tool available for human connectomics—high angular resolution diffusion imaging (HARDI). We review what is known about fcMRI and then explore fcMRI data reliability, effects of preprocessing, analysis procedures, and effects of different acquisition parameters across six studies (*n* = 98) to provide recommendations for optimization. Run length (2–12 min), run structure (1 12-min run or 2 6-min runs), temporal resolution (2.5 or 5.0 s), spatial resolution (2 or 3 mm), and the task (fixation, eyes closed rest, eyes open rest, continuous word-classification) were varied. Results revealed moderate to high test-retest reliability. Run structure, temporal resolution, and spatial resolution minimally influenced fcMRI results while fixation and eyes open rest yielded stronger correlations as contrasted to other task conditions. Commonly used preprocessing steps involving regression of nuisance signals minimized nonspecific (noise) correlations including those associated with respiration. The most surprising finding was that estimates of correlation strengths stabilized with acquisition times as brief as 5 min. The brevity and robustness of fcMRI positions it as a powerful tool for large-scale explorations of genetic influences on brain architecture. We conclude by discussing the strengths and limitations of fcMRI and how it can be combined with HARDI techniques to support the emerging field of human connectomics.

INTRODUCTION

The human brain is organized into parallel, interacting systems of anatomically connected areas. Understanding the functions of these systems and differences associated with atypical development and degenerative processes requires methods to measure connectivity and how it varies from one person to the next. Because of these needs, there has been great interest in developing techniques to measure connectivity in the human brain and to link the measured connectivity patterns to information about cytoarchitectonic boundaries and functional response properties. The present paper focuses on one such technique—functional connectivity MRI (fcMRI)—that provides indirect information about structural connectivity patterns that define brain systems.[1]

Expanding on related approaches (e.g., Friston 1994; Friston et al. 1993; Gochin et al. 1991; Horwitz et al. 1984; McIntosh 1999; Nunez et al. 1997), fcMRI is based on the observation that brain regions show slow, spontaneous fluctuations when measured using blood-oxygenation-level-dependent (BOLD) imaging methods (Biswal et al. 1995). Regions within anatomically connected brain systems, such as the motor and visual systems, are strongly and selectively correlated, suggesting the potential to use such correlations to infer the anatomic connectivity of brain systems. The present paper reviews the theory and methods of fcMRI (including its limitations) and then presents the results of six novel empirical studies that characterize parameters for its optimal use.

Functional connectivity MRI and its relation to alternative techniques

Until recently, the majority of information about the anatomic connectivity of the human brain came from studies of non-human primates using invasive tracing techniques (Felleman and Van Essen 1991; Jones and Powell 1970; Mesulam 2000; Ungerleider and Haxby 1994) and inferences from human brain lesions (e.g., Geschwind 1965). Postmortem tracing techniques in humans are feasible but have met with limited success because they are only able to trace connections spanning short distances (e.g., Burkhalter et al. 1993). For these

---

[1] Functional connectivity is operationally defined as temporally correlated remote neurophysiological events (Friston 1994; see also Horwitz 2003) and does not explicitly require that one event is influencing the other (e.g., 2 physiological events can be correlated because they are triggered by common stimulus or neuromodulatory events). The term effective connectivity is often evoked when the correlated events can be demonstrated to arise from a direct influence. While we adopt the agnostic term functional connectivity MRI (fcMRI) in this paper, accumulating evidence suggests that intrinsic activity correlations observed by fcMRI analysis are constrained by anatomic connectivity and may be a viable tool for making inferences about stable organizational properties of neural systems. fcMRI acquired at rest is also sometimes referred to as resting state fMRI (R-fcMRI) or discussed in terms of the networks it identifies—resting state networks (RSNs).

reasons, noninvasive human techniques based on MRI have become a focus for development even through significant technical hurdles present limitations on resolution and sensitivity.

Two main sets of MRI techniques are commonly used for noninvasive mapping of human brain connectivity: diffusion-based methods including diffusion tensor imaging (DTI) and high angular resolution diffusion imaging (HARDI) and indirect methods based on functional correlations including fcMRI. Additional methods based on measuring the distant effects of neural stimulation have also been applied successfully but are not as common (Pascual-Leone et al. 2000; Paus et al. 1997).

Diffusion-based methods exploit the property that water molecules move along white-matter bundles faster than they do against them. By measuring water diffusion in multiple directions, the location and trajectories of axonal bundles can be estimated and the pathways reconstructed using MRI (Basser et al. 2000; Conturo et al. 1999; Le Bihan et al. 2001; Mori et al. 2002). The major strength of diffusion techniques is that they directly measure anatomic structure. A limitation is their inability to resolve complex fiber organization, such as crossing fibers. This limitation has been partially overcome by advances in HARDI techniques including diffusion spectrum imaging (DSI) and Q-Ball methods (Tuch et al. 2002; Wedeen et al. 2005) and by advanced tractography algorithms such as those based on probabilistic estimates (Jbabdi et al. 2007). Nonetheless, currently applied diffusion techniques sometimes fail to detect known pathways, suggesting they are prone to type-II errors (e.g., Sherbondy et al. 2008).

Connectivity techniques based on functional correlation offer an orthogonal set of strengths and weaknesses when compared with diffusion techniques, a point we will return to in the discussion. Functional connectivity is based on the observation that distant brain regions often show strong correlations in their activity levels. Originally observed using positron emission tomography (PET) measures of between-subject variation (e.g., Horwitz et al. 1984; see Vogt et al. 2006 for an interesting recent application), functional correlations between widely distributed brain regions are consistently observed in analyses of fMRI time series data (see Fox and Raichle 2007 for review). As Friston (1994) noted in his comprehensive exposition of functional connectivity, the many repeated scans that can be acquired in quick succession with fMRI provide a rich source of information about correlated activity fluctuations.

Biswal et al. (1995) were the first to demonstrate the potential of fcMRI using intrinsic activity correlations. They showed that the BOLD signal time course from a region in the motor cortex was strongly correlated with the contralateral motor region and midline regions within the motor system. The coherent fluctuations were readily observed within individual participants, indicating that the method is highly sensitive and raising the possibility of measuring individual differences. Figure 1 displays a replication of the functional correlations demonstrated by Biswal et al. (1995) in a single participant. A high correlation between left and right motor cortices is evident as is minimal correlation between motor cortex and visual cortex, demonstrating the specificity of functional correlation measures. Unlike earlier approaches to functional connectivity that focused on stimulus-evoked modulations, the correlated fluctuations ob-
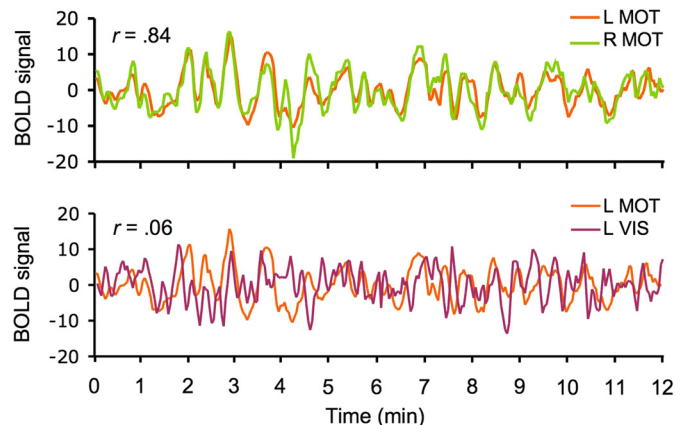

FIG. 1. The basis of functional connectivity MRI (fcMRI). Low-frequency spontaneous fluctuations in the blood-oxygenation-level-dependent (BOLD) signal are correlated over time between regions within the same brain systems. Examples from a single subject depict correlated spontaneous fluctuations between left and right motor cortex (*top*) and the absence of correlation between motor and visual regions (*bottom*). fcMRI methods make use of the selective correlations between regions to map the organization of brain systems. L, left; R, right; MOT, motor cortex; VIS, visual cortex.

served by Biswal et al. (1995) were manifest while participants rested passively without any detectable movement, suggesting the fluctuations were driven by intrinsic activity events constrained by anatomy. Reinforcing this possibility, Koch et al. (2002) combined diffusion-based and resting-state functional methods to provide initial evidence that BOLD signal correlations between regions are mediated by direct and indirect anatomic projections.

Properties of functional connectivity MRI

Since the seminal observation of Biswal and colleagues, multiple functional systems have been demonstrated to exhibit correlated fluctuations at rest including the visual and auditory systems (Cordes et al. 2000; Damoiseaux et al. 2006; De Luca et al. 2006; Hunter et al. 2006; Lowe et al. 1998; Van de Ven et al. 2004), the default network and the medial temporal lobe memory system (Buckner et al. 2008; Fox et al. 2005; Fransson 2005; Fransson and Marrelec 2008; Greicius et al. 2003, 2004; Vincent et al. 2006), the language system (Hampson et al. 2002), the dorsal attention system (Fox et al. 2005, 2006), and the frontoparietal control system (Vincent et al. 2008). Several reports have used data-driven approaches based on independent component analysis (ICA) to define multiple large-scale systems with a considerable degree of consistency between datasets (Beckmann et al. 2005; Damoiseaux et al. 2006; De Luca et al. 2006; Smith et al. 2009). Analyses targeting limbic and subcortical structures including the cingulate (Margulies et al. 2007), hippocampal formation (Kahn et al. 2008), thalamus (Zhang et al. 2008), striatum (Di Martino et al. 2008), amygdala (Roy et al. 2009), and the cerebellum (Habas et al. 2009; Krienen and Buckner 2009; O'Reilly et al. 2009) have demonstrated segregated pathways.

While the preceding studies were primarily based on correlated BOLD fluctuations that emerge spontaneously during awake rest, functional networks also show synchronous fluctuations during task paradigms and in varied states of consciousness. For instance, the sensory-motor system shows spontaneous correlation during rest (Biswal et al. 1995) and,

under certain conditions, increased correlation during finger tapping (Newton et al. 2007; but see Amann et al. 2009). The default network shows strong correlations during task conditions but at an attenuated level relative to rest (Fransson 2006). Spontaneous correlations persist during sleep (Fukunaga et al. 2006; Horovitz et al. 2008, 2009; Larson-Prior et al. 2009) and anesthesia (Greicius et al. 2008; Vincent et al. 2007), suggesting they reflect, to a large degree, intrinsic processes. Stage of sleep (Horovitz et al. 2009) and level of sedation (Vincent et al. 2007; see their supplementary materials) modulate intrinsic activity correlations, suggesting that state affects functional connectivity results. The common procedure of measuring synchronous fluctuations at rest does not imply that rest states have a special status that maximizes the presence of coherent fluctuations in all systems. However, because spontaneous fluctuations are often measured at rest, the method is frequently referred to as "resting state" fcMRI (R-fcMRI) and the identified brain networks as "resting state networks" (RSNs). Measurement during rest or passive fixation has the advantage of minimizing task-evoked BOLD fluctuations and is quite simple to implement.

The observation that spontaneous correlations are present ubiquitously across brain systems and persist in multiple states of consciousness raises the question of their origin and, specifically, whether they provide indirect information about anatomical connectivity (see Damioseaux and Greicius 2009 for review). Functional correlations between cortical regions might arise from common neuromodulatory input from ascending neurotransmitter systems or thalamo-cortical afferents (Friston 1994).

Several lines of evidence indicate that intrinsic BOLD fluctuations are constrained by anatomic connectivity. First, patterns of spontaneous synchronous fluctuations in the oculomotor system of the macaque monkey show high overlap with both evoked responses during an eye-movement task and with an anatomical network revealed by retrograde tracer injections into the lateral intraparietal area of the oculomotor system (Lewis and Van Essen 2000; Vincent et al. 2007). Margulies et al. (2009) recently demonstrated correspondance between functional connectivity and monkey tracer injections for four distinct pathways. Second, cortico-cortical axonal pathway densities among regions covering the entire cortex (as measured with diffusion-based imaging) show a significant (but not perfect) relationship to the strength of spontaneous functional correlations among those same regions (Hagmann et al. 2008; Honey et al. 2009). Third, in a case study where spontaneous correlations were assessed before and after a child underwent complete resection of the corpus callosum for the treatment of intractable epilepsy, a significant loss of interhemispheric BOLD correlations occurred while intrahemispheric correlations remained unchanged suggesting white-matter tracts were the conduits for functional correlations (Johnston et al. 2008).

However, there is also evidence that functional connectivity is not merely a reflection of direct structural connections and should not be considered an exact proxy for invasive tracing techniques or human diffusion-based methods. First, while fcMRI results are broadly consistent between passive and active task states, performance of a task can induce regional variation in correlation strengths indicating that functional connectivity can be modulated despite unchanged structural connectivity (Buckner et al. 2009; Fransson 2006; Hampson et al. 2002, 2004; Hasson et al. 2009; Newton et al. 2007; see also Friston 1994 for an early discussion

of the importance of modulating functional connectivity). Providing further evidence for state-dependent influences, several studies have modulated intrinsic activity correlations by manipulating task conditions prior to the rest data epoch (Albert et al. 2009; Hasson et al. 2009; Lewis et al. 2009; Waites et al. 1995) suggesting important components of intrinsic activity may be linked to consolidation. Second, functional connectivity exists between regions that do not display direct anatomic connectivity including right and left primary visual cortex (Vincent et al. 2007) and between the hippocampal formation and certain regions of the dorsal medial prefrontal cortex (Fransson and Marrelec 2008; Greicius et al. 2009). These correlations likely reflect polysynaptic connections or common feed-forward projections (from the lateral geniculate nucleus in the instance of primary visual cortex). These collective observations place constraints on interpretation of fcMRI data and suggest limitations of the technique. Several recent mathematical models have begun to explore neural dynamics and propagation properties that might form the basis of intrinsic activity correlations at slow time scales (e.g., Deco et al. 2009; Ghosh et al. 2008; Honey et al. 2007).

A particularly clear demonstration that functional correlations are constrained by anatomy and also that they reflect polysynaptic connections arises from the study of cerebro-cerebellar circuits (Allen et al. 2005; Habas et al. 2009; Krienen and Buckner 2009; O'Reilly et al. 2009). The cerebro-cerebellar system is an excellent target because its long-range polysynaptic connections are characterized by three relevant properties. First, cortical regions project to the *contralateral* cerebellum via the pons and afferents that cross through the deep cerebellar nuclei and the thalamus. Second, direct projections do not exist between the cerebral cortex and the cerebellum; they must traverse either one (efferents) or two (afferents) synapses. Finally, cerebro-cerebellar connections are organized as closed, independent circuits. Cortical regions receive input from the same cerebellar regions that they project to (Kelly and Strick 2003; Middleton and Strick 2000). This polysynaptic connectional architecture is thus well suited to test the specificity of fcMRI.

Using cerebro-cerebellar circuitry as the target, Krienen and Buckner (2009) observed correlations between motor regions with predicted anterior portions of the cerebellum. Most notably, robust correlations were also observed between anatomically distinct regions of the cerebellum and regions of prefrontal cortex (see also Habas et al. 2009; O'Reilly et al. 2009). Prefrontal correlations appeared in Crus I and Crus II of the cerebellum (Schmahmann et al. 1999, 2000). Using viral tracing studies in the monkey, these cerebellar regions have been shown to project to prefrontal cortex area 46 (Kelly and Strick 2003). The cerebellar connectivity also showed the expected crossed-lateralization in relation to the cerebral cortex with the BOLD fluctuations in the right neocortex preferentially correlated with the left cerebellum and vice versa. These results provide strong evidence that spontaneous BOLD fluctuations are constrained by anatomical projections. It is especially compelling in the instance of cerebro-cerebellar circuits as the contralateral connectivity pattern cannot be attributed to artifacts such as shared vasculature (the cerebellum is supplied by its own major arteries) or head motion. As there are no direct anatomic projections between the cerebral cortex and cerebellum, the results indicate that fcMRI reflects polysynaptic ana-

tomic connectivity or correlation patterns that emerge from common inputs.

Analysis of network properties and graph theory

The major use of fcMRI to date has been to identify functional connectivity patterns within and between distinct brain systems. As discussed in the preceding text, tremendous strides have been made through application of fcMRI in this manner. There has also been a recent expansion of fcMRI analysis to include examination of more global properties and metrics of connectivity (see Bullmore and Sporns 2009 for review).

Neuroanatomists have long recognized that convergence of information is a particular challenge for neural circuitry because it opposes the pressure to segregate information processing across specialized brain systems (Jones and Powell 1970; Mesulam 1998; Pandya and Kuypers 1969). The anatomic connectivity of the cerebral cortex reflects these opposing demands with certain areas processing highly specialized types of information (e.g., the visual and auditory systems) and other heteromodal association areas serving as integration zones. Mesulam (1998), in a detailed analysis of the issue, referred to these convergence zones that link distributed sources as "hubs" and "nexuses." A particularly important recent expansion of fcMRI has been to offer insight into the global organizational properties that allow brain networks to efficiently segregate and integrate information processing. The explorations have relied heavily on graph theory.

The mathematical field of graph theory allows abstract properties of complex systems, such as brain systems, to be quantitatively characterized and mapped. In doing so, simple metrics can be derived that capture the global tendencies that define normal brain architecture and its variability among subjects. Local (region-by-region) topological properties can also be obtained such as whether individual regions serve as hubs. Within this approach, the organization of the human brain is formally modeled as a complex system with small world properties (Bassett and Bullmore 2009; Bullmore and Sporns 2009; Watts and Strogatz 1998). Functional and structural connectivity between brain regions are examined to determine whether there are orderly sets of regions that have particularly high local connectivity (forming families or clusters) as well as limited numbers of regions that serve as relay stations or hubs (Sporns et al. 2007). Network properties that include small world features are found in many complex biological and social systems and are believed to increase efficiency of signal propagation and/or communication (for reviews, see Bassett and Bullmore 2006; Bullmore and Sporns 2009; Rubinov and Sporns 2009).

For example, recent investigations have applied graph theory to fcMRI data by examining functional connectivity between numerous pairs of regions in the cerebral cortex to determine whether there are hubs of connectivity (Achard et al. 2006; Buckner et al. 2009), paralleling earlier analyses of invasive tract tracing (Sporns et al. 2007) and diffusion-based (Hagmann et al. 2008) data. What has emerged from the fcMRI investigations is a map of the heteromodal cortical regions that are nexuses of connectivity defined specifically by their disproportionate tendency to have high numbers of widespread cortical connections (Buckner et al. 2009). Hubs may function

to minimize wiring and metabolism costs by providing a limited number of distant connections that integrate local networks (Bassett and Bullmore 2006). Relevant here is the potential of graph theoretical analysis to characterize global and local properties of brain networks in ways that are not captured by focusing on individual brain systems (e.g., rest-state networks) or distinct patterns of connectivity.

As another example, Fair et al. (2009) combined fcMRI and graph theory to show that functional connectivity within a frontoparietal network is present in early childhood but that connection strength continues to develop with increasing age, thereby indicating that fcMRI may make it possible to track microstructural maturation during development (see also Fair et al. 2008; Kelly et al. 2009). In addition, their results indicate that reductions in short-range connections occur with a concomitant strengthening in long-range connections, potentially caused by synaptic pruning and increased myelination of long-range fibers (Fair et al. 2007a). One might imagine that disturbances of brain function in neuropsychiatric developmental disorders (e.g., autism and schizophrenia) could arise from general tendencies to over- or under-connect networks throughout the brain in addition to disturbances that affect particular systems.

Clinical applications

Potential clinical applications of fcMRI emerged shortly after the development of the technique in normal participants (Haughton and Biswal 1998). The most basic idea is to use the strength of correlations between functionally coupled regions as a marker of brain system integrity. This approach has been surprisingly powerful for detecting differences in neurological and psychiatric disorders. In a particularly influential demonstration, Greicius et al. (2004) showed that functional connectivity within the default network is disrupted in patients with Alzheimer's disease (AD) as compared with normal older controls (see also Sorg et al. 2007; Wang et al. 2007). Connectivity disruptions were further detected in mild cognitive impairment (MCI) (Zhou et al. 2008) and in cognitively normal older individuals who harbor the pathology of AD (Hedden et al. 2009; Sheline et al. 2009). These observations indicate that the method is sensitive and of potential diagnostic value.

Functional disruption has now been reported for a number of neuropsychiatric disorders including autism (Cherkassky et al. 2006; Kennedy and Courchesne 2008), attention deficit hyperactivity disorder (Uddin et al. 2008), depression (Anand et al. 2005, 2009; Greicius et al. 2007), and schizophrenia (Bluhm et al. 2007; Garrity et al. 2007; Whitfield-Gabrieli et al. 2009; Zhou et al. 2007; see Calhoun et al. 2009; Greicius et al. 2008 for reviews). Typical aging in the absence of disease has also been demonstrated to correlate with changes in functional connectivity (Andrews-Hanna et al. 2007; Damoiseaux et al. 2008; Meunier et al. 2009). On the one hand, the detection of dysfunction across a wide range of disorders and in aging suggests the technique is highly sensitive. On the other hand, the generality of detectable deficits raises the question of whether disruption of large-scale brain systems is a common outcome of many underlying processes and, ultimately, whether fcMRI will be sufficiently specific to be clinically useful. This is an open question. In a provocative recent study, Seeley et al. (2009) showed that distinct degenerative neurological diseases including AD, semantic dementia, and frontotemporal demen-

tia show network disruption that maps to distinct brain systems defined by fcMRI.

Another class of clinical application for fcMRI is in presurgical planning. Treatments for epilepsy and brain tumors may involve the neurosurgical removal of brain tissue. Maps of the locations of functioning brain systems and knowledge about the lateralization of language function in individual patients are critical information that allows the surgeon to maximize the size of the resection while minimizing the damage to eloquent cortex. Two independent groups have recently demonstrated the feasibility of mapping functional systems in preoperative patients using fcMRI (Liu et al. 2009a; Shimony et al. 2009). Of importance, presurgical mapping using fcMRI can be performed while participants are at rest or under light anesthesia. In addition, given that multiple brain systems have been demonstrated to be lateralized using fcMRI (e.g., Fox et al. 2006; Liu et al. 2009b; H. Yan et al. 2009), fcMRI-enabled presurgical mapping has the potential to replace more invasive alternatives for determining language lateralization.

Physiological noise, anticorrelations, and optimization

There are several methodological issues associated with the application of fcMRI that merit further research and clarification. For example, despite remarkable stability of functional connectivity estimates across studies, formal tests of reliability of fcMRI measures have been scarce. Shehzad et al. (2009) reported moderately high reliability in a systematic investigation of within- and between-subject reliability. Their results further demonstrated that the strongest correlations were also the most reliable, positive correlations were more reliable than negative correlations, and mean correlations computed at the group level exhibited higher reliability than within-subject correlations consistent with the increased signal-to-noise levels afforded by signal averaging. However, Honey et al. (2009) raised questions about fcMRI reliability by comparing the correlation strengths for large numbers of region pairs between multiple data sets in the same subject. They found low to moderate reliability within subjects (e.g., $r = 0.38$ to $r = 0.69$). In a recent study, Meindl et al. (2009) reported high reproducibility of core components of the default network across three scan sessions but lower reproducibility of correlations for superior frontal gyrus. Moreover they showed that reproducibility between sessions was comparable to scans acquired within the same session. Liu et al. (2009b) observed moderate within-subject correlations across sessions for fcMRI estimates of brain asymmetries ($r = 0.58$ to $r = 0.79$). Zuo et al. (2009) recently showed moderate to high reliability of amplitude measures of spontaneous low-frequency fluctuations on which fcMRI estimates are based.

Another issue is that raw BOLD signal time courses are noisy due to scanner artifacts, participant motion, and physiological sources such as cardiac and respiratory cycles. As a result of the need to reduce spurious noise, multiple processing steps are typically conducted to increase signal to noise (e.g., spatial smoothing), isolate signal components most relevant to fcMRI (e.g., temporal filtering), and remove signal contributions from motion and physiological noise (e.g., through regression of white-matter, ventricle, and whole-brain signals). Each of these steps raises potential interpretative issues and opportunities for methodological optimization.

The BOLD fluctuations that most consistently produce correlations within functional networks occur within a range of 0.01–0.08 Hz, corresponding to a cycle repetition time of 12.5–100 s (Biswal et al. 1995; Cordes et al. 2000; De Luca et al. 2006; Fransson and Marrelec 2008; Lowe et al. 1998; Wu et al. 2008; Zuo et al. 2009). Therefore the signals of interest are in the low-frequency spectrum and application of a low-pass filter (e.g., retaining frequencies <0.1 Hz) as a preprocessing step is aimed at removal of higher frequencies. However, a low-pass filter will not be effective in removing signals faster than the Nyquist frequency (equal to half of the sampling rate) and slower than the band-pass cut-off, which may be aliased into the retained frequency spectrum. In this respect physiological noise, especially low-frequency components related to respiration, is a particular concern (Birn et al. 2006, 2008a,b; Chang et al. 2009; Shmueli et al. 2007; Van Buuren et al. 2009; Wise et al. 2004). While breath-to-breath effects occur with a frequency of ~0.3 Hz and are possibly removed by the band-pass filter, variations over time in breathing rate typically occur at much slower frequencies (~0.03 Hz) (Birn et al. 2006). These sources of noise may have a global effect across the brain and inflate estimated correlations between brain regions if not properly addressed. Without addressing global influences, fluctuations across all regions tend to show positive correlation even between regions unlikely to be anatomically or functionally connected (e.g., primary visual and primary auditory cortex).

Several ways to minimize unwanted physiological variation from BOLD data have been proposed. Some methods utilize fast sampling rates (e.g., TR < 250 ms) at the expense of brain coverage when using conventional BOLD sequences (Chuang and Chen 2001). Other methods use postprocessing to isolate cardiac and respiratory signals (simultaneously recorded during image acquisition) and incorporate these signals as null regressors in fcMRI analytic models (Birn et al. 2008b; Chang and Glover 2009a,b; Chang et al. 2009; Glover et al. 2000; Lund et al. 2006). Additional commonly used null regressors in fcMRI analyses include signals averaged over the ventricles, the deep cerebral white matter, and the whole brain (global signal).

Removal of signal from the ventricles and white matter is motivated by the fact that these regions contain a relatively high proportion of noise caused by the cardiac and respiratory cycles (Dagli et al. 1999; De Munck et al. 2008; Lund et al. 2006; Windischberger et al. 2002). Furthermore, it is assumed that physiological sources will cause the same pattern of activity over time in affected voxels of the brain (although not necessarily at the same magnitude) (Macey et al. 2004). One way to counteract these global effects is by regression of the whole-brain signal, a method also referred to as "regression of the global signal," "global signal normalization," or "orthogonalization of the global signal."

The use of whole-brain signal regression has presented challenging interpretive issues. The whole-brain signal is defined as the time course of the average signal intensity within the brain and is typically removed by regression from each voxel's time series, after which the residual time series are used for further analysis (Desjardins et al. 2001). This method of removal of the whole-brain signal has recently been the subject of scrutiny because, in addition to its intended purpose of removing noise, whole-brain signal regression is associated

with the emergence of robust negative correlations (Murphy et al. 2009). There are two possible reasons for the emergence of negative correlations after whole-brain signal regression. First, as the method forces correlation strengths between a given source (e.g., a region of interest) and other voxels in the brain to be distributed around zero, negative correlations may emerge because the distribution of correlations is shifted (Buckner et al. 2008; Fox et al. 2009; Murphy et al. 2009; Vincent et al. 2006). Second, neurophysiologically meaningful negative correlations may only become detectable after the removal of nonspecific noise correlations (Chang and Glover 2009b; Fox et al. 2009).

Studies using task paradigms have previously noted that regression of the whole-brain signal has the potential to give qualitatively different results in GLM analyses, may reduce sensitivity (because task-related signal contributing to the whole-brain signal is regressed out), and may cause negative values to emerge (for discussion, see Aguirre et al. 1997; Desjardins et al. 2001). In the case of data collected at rest, we do not know exactly what proportion of the whole-brain signal represents neurophysiological signal or physiological noise. However, there is a strong association of breath-to-breath variation in the end-tidal partial pressure of carbon dioxide (PCO_2) with the whole-brain signal at rest (Wise et al. 2004) and during controlled manipulation of PCO_2 (Corfield et al. 2001). Thus regression of the whole-brain signal could provide a relatively simple approach to minimize the effects of PCO_2 variation, which is a predominant source of physiological noise in the BOLD signal (Chang and Glover 2009a; Wise et al. 2004). However, it is currently not known to what extent the whole-brain signal correlates with signals of true neurophysiological origin, or how activation of multiple coherent networks during rest may contribute to the whole-brain signal.

Fox et al. (2009) explored the question of whether global regression facilitates or impedes observation of neurally meaningful relationships by comparing correlation maps computed with and without global correction. Functional connectivity of several well-established cortico-thalamic systems were assessed, and it appeared that removal of the whole-brain signal improved overlap of the fcMRI results onto known systems. Weissenbacher et al. (2009) demonstrated that after whole-brain signal regression, specificity of functional connectivity maps of the motor system increased and spurious correlations between the motor and visual systems decreased. It is noteworthy that both Fox et al. (2009) and Weissenbacher et al. (2009) found only improvements (never decrements) due to whole-brain signal regression for systems expected to show *positive* correlations, leading Weissenbacher and colleagues to conclude that whole-brain signal regression is a viable preprocessing step but that one should refrain from interpreting negative correlations.

Although whole-brain signal regression mathematically mandates negative correlations in maps of individual study participants (Buckner et al. 2008; Fox et al. 2009; Murphy et al. 2009), the negative correlations are not constrained to a specific and consistent spatial distribution across participants. Therefore it remains an intriguing phenomenon that group level analyses consistently reveal robust negative correlations between regions placed within the default network and regions within the dorsal attention system (Fox et al. 2005, 2009; Fransson 2005; Kelly et al. 2008; Murphy et al. 2009; Uddin et

al. 2009). In contrast, regions in the visual cortex display a rather random spatial pattern of weak negative correlations that are most visible in maps using lenient thresholds (see Fig. 5 from Murphy et al. 2009).

Providing further insight into the effects of whole-brain signal regression, Chang and Glover (2009b) recently compared two methods of physiological noise removal: regression of the whole-brain signal and regression of derived models of the measured heart rate and breathing variability. They observed that negative correlations were present even when no whole-brain signal regression was performed. Furthermore regions of negative correlations that were observed prior to any noise correction increased their strength and extent after regressing out variability of heart rate and breathing (again, without application of whole-brain signal regression). Finally, regions showing negative correlation after regression of variability of heart rate and breathing overlapped those regions showing the greatest negative correlations after whole-brain signal regression. From these observations, Chang and Glover suggest that whole-brain signal regression may be useful for identifying candidate regions that show neurophysiological meaningful negative relationships but also that investigators should refrain from interpreting the magnitude of negative correlation coefficients following whole-brain signal regression.

Knowing if the negative correlations do reflect neurophysiological interactions is critically important because negative correlations (anticorrelations) between brain systems have been interpreted as evidence for an antagonistic relationship between systems (Fox et al. 2005; Fransson 2005). Such an observation, if valid, may be profoundly important for understanding information flow through cortical processing pathways and how incompatible processing streams resolve competition. The observation that negative correlations are robust only after whole-brain signal regression has been applied indicates that these results should be approached with caution. If the premise of antagonistic networks holds true, it will have far-reaching consequences for our thinking about the interplay of functional brain systems. As multimodal neuroimaging techniques continue to develop, they may provide an avenue for understanding whether negative correlations between brain systems have a neurophysiological origin. That is, the most compelling evidence for the presence of antagonistic relationships between large-scale systems will be to demonstrate and explore their neurophysiological origins outside the context of BOLD fMRI (see Popa et al. 2009 for an interesting advance in this direction).

Goals of the present paper

While fcMRI is not analogous to measurement of anatomical connectivity, accumulating evidence suggests it is sufficiently constrained by anatomy to allow distinct brain systems to be identified and individual differences to be characterized. Several interpretative issues will need further work, but the relative ease of data acquisition using a standard MR scanner under rest conditions positions fcMRI as a valuable tool for future research and possible clinical applications. The goal of the remainder of this paper is to provide empirical characterization of fcMRI analyses and acquisition procedures. fcMRI data reliability, effects of preprocessing, analysis procedures, and

effects of different acquisition parameters were explored across six studies ($n = 98$) to better understand the properties of fcMRI and to provide practical recommendations for optimization.

METHODS

Overview

The present studies explored factors that influence fcMRI and, in doing so, provide recommendations to optimize procedures for fcMRI data acquisition and analysis. Three objectives were pursued. First, we developed a metric to quantitatively measure the results of fcMRI analysis including an estimate of signal strength and also a reference estimate of spurious (noise) correlation. The signal metric consisted of the mean correlation strength in two a priori defined networks—the default network (default) and the dorsal attention system (attention). Noise correlations were estimated based on correlations between primary motor, auditory, and visual cortex as they typically show near zero correlations (reference). These metrics served as a means to assess signal and noise for all subsequent analyses.

Second, we explored the properties of typical analysis procedures as well as the reliability of fcMRI data. Preprocessing steps examined were spatial smoothing, temporal filtering, motion regression, whole-brain (global) signal regression, ventricle and white-matter signal regression, and respiratory signal regression. To foreshadow the results, commonly used preprocessing steps involving regression of nuisance signals minimize nonspecific (noise) correlations including those associated with respiration. However, negative correlations (anticorrelations) were present at the group level only after regression of the whole-brain signal. Reliability within pivotal functional networks was tested within- and between-subjects, and correlation maps were found to replicate across independent data sets. We also confirmed the comparability of outcomes from independent-component analysis (ICA) and seed-based analyses.

Finally, we conducted a series of experiments to examine the influence of different acquisition parameters on fcMRI. Run length (2–12 min), run structure (1 12-min run or 2 6-min runs), temporal resolution (2.5 or 5 s), spatial resolution (2 or 3 mm), and the task (fixation, eyes closed rest, eyes open rest, continuous word-classification) were varied. Functional connectivity estimates were found to be robust across most data-acquisition parameters but were influenced by the task performed during acquisition. The results of these studies provide estimates for optimization of fcMRI acquisition parameters as well as insight into the tradeoffs of various alternatives. As will be

shown, estimates of functional connectivity for two major networks (the default network and the dorsal attention system) stabilize rapidly over time, suggesting brief acquisitions are feasible and powerful for certain applications. Collectively, the results suggest that fcMRI represents a rapid and robust estimate of functional networks that is minimally affected by physiological noise (after appropriate data processing) and by most acquisition parameters.

Participants

Ninety-eight young adults participated for payment across six studies (age: 18–42, mean age of 23.3 ± 4.8) (see Table 1). All participants had normal or corrected to normal vision and were right handed. Participants with a history of neurological or psychiatric treatment as well as those using psychoactive medications were excluded. Informed consent was obtained in accordance with guidelines set forth by the institutional review board of Partners Healthcare Inc. A portion of the 3 Tesla rest data were included in a composite analysis that examined connectivity of heteromodal hubs (Buckner et al. 2009) and brain asymmetry (Liu et al. 2009b). Dataset 6 has been reported previously but not in the context of functional connectivity (Evans et al. 2009).

Image acquisition

Scanning was performed on a 3 Tesla TimTrio system (Siemens, Erlangen, Germany) using a 12-channel phased-array head coil for Datasets 1 through 5. Dataset 6 was acquired on a 1.5 Tesla Allegra system (Siemens) using the vendor's circularly polarized head coil. High-resolution three-dimensional (3D) T1-weighted magnetization prepared rapid acquisition gradient echo (MP-RAGE) anatomical images were collected with the following parameters TR = 2,530 ms, TE = 3.44 ms, FA = 7°, $1 \times 1 \times 1.33$ mm voxels (dataset 1), TR = 2,530 ms, TE = 3.44 ms, FA = 7°, $1 \times 1 \times 1$ mm voxels (datasets 2, 4, and 5), TR = 2,300 ms, TE = 2.98 ms, FA = 9°, $1 \times 1 \times 1.2$ mm voxels (dataset 3). TR = 2,730 ms, TE = 3.39 ms, FA = 7°, $1 \times 1 \times 1.33$ mm voxels (dataset 6).

Functional data were acquired using a gradient-echo echo-planar pulse sequence sensitive to BOLD contrast (Kwong et al. 1992; Ogawa et al. 1992). The TR, voxel size, and the number of runs per condition differed across studies (see Table 1). Transverse slices aligned to the AC-PC plane covered the whole brain except for datasets 3c and 6. Dataset 3c had a higher temporal resolution than its reference condition (dataset 3a), and to keep the other acquisition parameters constant (e.g., voxel size), a smaller portion of the brain

TABLE 1. *Overview of datasets*

Dataset	n	Mean Age, yr	Voxel Size, mm	TR, s	Duration, min*	Task
1 Reference dataset	48 (20)	22.3 ± 3.0	$3\times3\times3$	2.5	6.00 (2)	Fixation
2 Test of reliability across days	6 (3)	24.2 ± 3.2	$2\times2\times2$	5.0	5.10 (16[†])	Fixation
3 a Reference condition[#]	6 (3)	25.7 ± 3.5	$2\times2\times2$	5.0	6.00 (2)	Fixation
b Effect of run length			$2\times2\times2$	5.0	12.00 (1)	Fixation
c Effect of temporal resolution			$2\times2\times2$	2.5	6.00 (2)	Fixation
d Effect of spatial resolution			$3\times3\times3$	2.5	6.00 (2)	Fixation
e Effect of task			$2\times2\times2$	5.0	6.00 (2)	Eyes closed rest
4 a Effect of task[#]	12 (6)	21.3 ± 1.8	$3\times3\times3$	3.0	6.57 (3)[§]	Fixation
b						Eyes closed rest
5 a Effect of task[#]	16 (4)	21.1 ± 2.5	$3\times3\times3$	3.0	5.00 (2)[§]	Eyes closed rest
b						Fixation
c						Eyes open rest
d						Semantic classification task
6 Effect of respiration	10 (6)	33.2 ± 6.7	$6\times3\times3$	4.0	6.00 (1)	Eyes open rest

Values are means ± SD. Number of males is in parentheses in second column; number of runs is in parentheses under duration. *Duration reflects the time for each individual run and does not include initial images discarded to allow for T1 stabilization. The total data-acquisition time is the duration multiplied by the number of runs. Note that all total data-acquisition times were held constant for dataset 3. [†]Dataset 2 involved 8 runs collected on two separate days for a total of 16 runs per subject. [#]Order of conditions was counterbalanced between subjects. [§]Datasets 4 and 5 involved 3 and 2 runs per task condition, respectively.

was scanned that included the most critical regions of interest for testing fcMRI (see *Definition of signal and reference networks* for details). TE was 30 ms for all acquisitions at 3 Tesla (datasets 1–5). Dataset 6 employed a longer TE (40 ms) and was acquired in sagittal slices as part of a separate study explicitly designed to investigate neural activity associated with breathing at rest (Evans et al. 2009). The FA was 90° for all datasets. Head motion was restricted using a pillow and foam inserts that surrounded the head. Earplugs were used to attenuate scanner noise.

Visual stimuli were generated using an Apple PowerBook G4 (Apple, Cupertino, CA) running Psychtoolbox (Brainard 1997) within Matlab (The Mathworks, Natick, MA) and projected onto a screen positioned at the head of the magnet bore.

Data preprocessing

A series of preprocessing steps was conducted that are common to most fMRI analyses. The first four volumes of each run were discarded to allow for T1-equilibration effects. Slice-acquisition-dependent time shifts were corrected per volume (SPM2, Wellcome Department of Cognitive Neurology, London, UK). Then rigid body translation and rotation were used to correct for head motion (Jenkinson et al. 2002) (FMRIB, Oxford, UK), and atlas registration was achieved by computing affine and nonlinear transforms connecting the first volume of the functional run using SPM2, with a T1 EPI template in the Montreal Neurological Institute (MNI) atlas space (Evans et al. 1993). Data were resampled to 2-mm isotropic voxels and spatially smoothed using a 6-mm full-width half-maximum (FWHM) Gaussian kernel.

Next a series of preprocessing steps specific to fcMRI analysis were performed. Temporal (band-pass) filtering removed constant offsets and linear trends over each run while retaining frequencies <0.08 Hz, and the mean signal intensity over the run was removed. Several sources of spurious or regionally nonspecific variance were removed by regression of nuisance variables including six parameters obtained by rigid body head motion correction, the signal averaged over the whole brain (global signal), the signal averaged over the lateral ventricles, and the signal averaged over a region centered in the deep cerebral white matter. Temporally shifted versions of these waveforms were also removed by inclusion of the first temporal derivatives (computed by backward differences) in the linear model. This regression procedure removes variance unlikely to represent regionally specific correlations of neuronal origin. Regression of each of these signals was performed simultaneously and the residual volumes were retained for the fcMRI analysis.

To formally explore the effects of the chosen preprocessing steps on connectivity analysis, we also conducted a specific set of analyses to measure the influence of each sequential step on signal properties. As the results will reveal, the implemented preprocessing steps represent a reasonable and powerful approach to fcMRI data analysis. However, certain preprocessing steps have consequences that must be considered carefully. Whole-brain signal regression, for example, is associated with a shift of the distribution of correlation coefficients (Buckner et al. 2008; Fox et al. 2009; Murphy et al. 2009; Vincent et al. 2006).

Finally, one assumption of these preprocessing steps is that regression of the nuisance variables, in particular the whole-brain signal regression, removes unwanted physiological signals including those induced by respiration (Birn et al. 2006; Wise et al. 2004). Dataset 6 measured respiration and tested this assumption directly.

Correlation maps and correlation between regions

Maps of functional connectivity were obtained by computing the correlation between the mean signal time course from voxels within a specific region of interest (ROI) and the time courses from all acquired voxels using Pearson's product moment correlation. Corre-

lation maps were converted to z-maps using Fisher's r-to-z transformation (Zar 1996). This transformation increases normality of the distribution of correlations in the sample. Group maps were computed by averaging individual $z(r)$ correlation maps. Maps of functional connectivity were used to illustrate connectivity networks as well as overlap for the same networks between subjects, sessions, and datasets.

To quantify functional connectivity, correlation strengths between a priori ROIs were computed by extracting the time course from the mean of all voxels included within each region. Pearson's correlation was then computed between the time courses from each pair of regions and normalized using Fisher's r-to-z transformation. For most analyses, correlations between multiple pairs of regions within well-studied networks were used as the central metric as described in the next section.

Definition of signal and reference networks

A set of quantitative metrics were developed that could be used to assess improvements and degradations in fcMRI. We employed a practical approach. We used dataset 1, which contained a large sample of subjects ($n = 48$) with high signal to noise, to define a set of expected correlations between regions within known networks (the default network and the dorsal attention system) as well as a reference set of regions that do not typically show correlation (between visual, auditory, and motor regions). The correlations within the known networks were operationally designated as "signal" and the spurious correlations between the reference regions as "noise." We then carried these networks forward to explore the various analysis procedures and acquisition options, always asking the same question of whether a procedure enhanced the ability to detect the signal networks and minimized spurious correlations between the reference regions.

The two signal networks selected for analysis were the default network (Buckner et al. 2008; Fox et al. 2005; Fransson and Marrelec 2008; Greicius et al. 2003; Raichle et al. 2001) and the dorsal attention system (Corbetta and Shulman 2002; Fox et al. 2005, 2006). Each of these networks has multiple, bilateral regions that show strong correlation with one another and also strong negative correlation for regions between the networks (e.g., Fox et al. 2005; Fransson 2005), at least insofar as typical preprocessing steps that include whole-brain regression are performed (Murphy et al. 2009). Figure 2 shows the regions that were included in each network, which will be referred to as the default, attention, and reference networks throughout. Atlas coordinates of the center of each region use the MNI coordinate system (Evans et al. 1993) and all created regions had a radius of 4 mm. The time course was averaged across the voxels from both hemispheres in cases of bilateral regions.

Regions within the networks were defined in the following manner. A correlation map was computed using an initiating seed region in the posterior cingulate cortex (pC) based on a previous study (Andrews-Hanna et al. 2007) (MNI Coordinate 0, −53, 26). Although the coordinates of this initial pC seed region are somewhat arbitrary, similar results were obtained using other pC coordinates from the literature. The pC plays a central role in the default network (Buckner et al. 2008; Fransson and Marrelec 2008), and the resulting correlation map was used to identify peak voxels of well-established nodes of the default network: medial prefrontal cortex (mPFC: 0, 52, −6), lateral parietal cortex (LatPar: −48, −62, 36; 46, −62, 32), and hippocampal formation (HF: −24, −22, −20; 24, −20, −22). Because the pC is a major hub in the default network, a time course extracted from the pC was expected to be negatively correlated with regions that are part of the dorsal attention system (Fox et al. 2005). Therefore we defined the center of well-established nodes of the dorsal attention system as negative peaks in the pC seed correlation maps: intraparietal sulcus (IPS: −24, −58, 52; 22, −58, 54), frontal eye fields (FEF: −38, −4, 48; 40, −4, 48), and medial temporal area (MT+: −56, −60, −2; 54, −58, −4). Again alternative methods for defining the dorsal attention
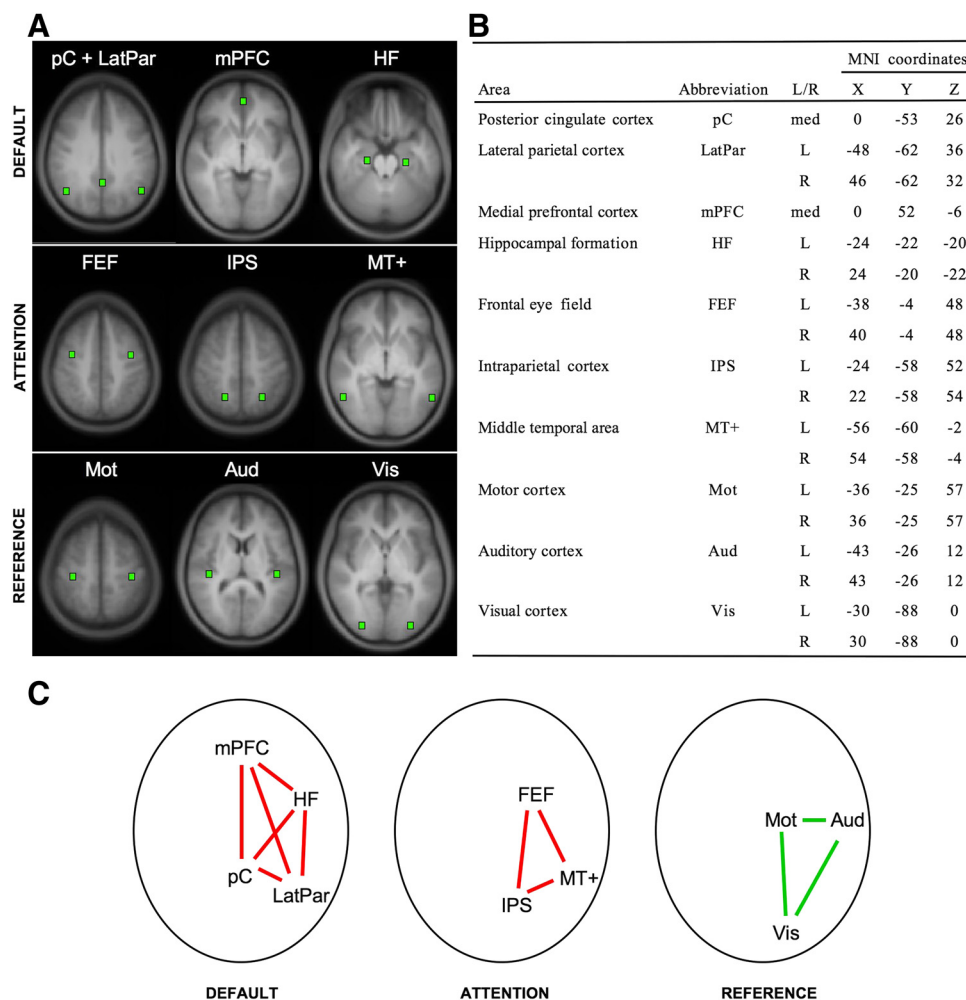
A

DEFAULT: pC + LatPar | mPFC | HF
ATTENTION: FEF | IPS | MT+
REFERENCE: Mot | Aud | Vis

B

Area	Abbreviation	L/R	MNI coordinates		
			X	Y	Z
Posterior cingulate cortex	pC	med	0	-53	26
Lateral parietal cortex	LatPar	L	-48	-62	36
		R	46	-62	32
Medial prefrontal cortex	mPFC	med	0	52	-6
Hippocampal formation	HF	L	-24	-22	-20
		R	24	-20	-22
Frontal eye field	FEF	L	-38	-4	48
		R	40	-4	48
Intraparietal cortex	IPS	L	-24	-58	52
		R	22	-58	54
Middle temporal area	MT+	L	-56	-60	-2
		R	54	-58	-4
Motor cortex	Mot	L	-36	-25	57
		R	36	-25	57
Auditory cortex	Aud	L	-43	-26	12
		R	43	-26	12
Visual cortex	Vis	L	-30	-88	0
		R	30	-88	0

C

DEFAULT: mPFC, HF, pC, LatPar
ATTENTION: FEF, MT+, IPS
REFERENCE: Mot — Aud, Vis

FIG. 2. Definition of seed regions and networks used for analysis. The analyses in the present paper used a common set of seed regions and networks (see METHODS) that are illustrated here. The default network (default) and the dorsal attention system (attention), two brain networks commonly reported in the literature, were used to measure functional connectivity signal strength. A set of regions within primary motor, visual, and auditory cortex that do not typically show correlation were used as a reference (reference). *A*: locations of regions of interest (ROIs) are overlaid on the averaged anatomical scan of all subjects from dataset 1. All image sections and atlas coordinates here and elsewhere are referenced to the Montreal Neurological Institute (MNI) coordinate system (Evans et al. 1993). *B*: the ROIs with their abbreviation, laterality, and coordinates are listed. *C*: schematic representations of the default, attention, and reference networks. The mean correlation among default network regions and, separately, among attention network regions are expected to be high and positive (red lines). The mean correlation among reference regions is expected to be near 0 (green lines). The mean correlations in the default, attention, and reference regions were used as the dependent measures in the present paper to determine the influences of various paradigm and processing manipulations on functional connectivity analysis. Left is displayed on the left. Med, medial. For display purposes, in case of bilateral regions, only the right region is shown in *C* although the BOLD signal was averaged across the ROIs from both hemispheres.

system are possible. In our initial explorations, these yielded comparable regions, so we selected this approach based on Fox et al. (2005).

In addition to identifying regions that contribute to the signal networks, we also selected a number of reference ROIs from brain regions among which correlations over time are typically not expected: motor cortex (Mot: ± 36, -25, 57), visual cortex (Vis: ± 30, -88, 0), and auditory cortex (Aud: ± 43, -26, 12). Moreover, to obtain an estimate of noise in pC seed correlation maps for datasets 1 and 3, a mask was created by taking the average pC seed correlation map thresholded to include only regions with low correlations (*z* values between -0.12 and 0.12). The absolute mean value of correlations with the pC seed regions within this mask was computed for each subject (the mask for dataset 3 is shown in Fig. 11*B, inset*).

The same seed regions were used for all analyses with the exception of dataset 3. For this dataset, the regions were defined using identical methods as described in the preceding text with the exception that the initial pC seed (0, -56, 26) correlation map was an average of the 30 maps that equally weighted all participants and conditions contributing to the analysis (i.e., 1 map for each participant and condition). The resulting ROIs were thus tailored to this specific dataset and ensured that all conditions contributed equally to the definition of the ROIs and that the ROIs were not biased toward giving higher correlations in one condition compared with another. Using this procedure, the following coordinates were defined for dataset 3: mPFC (2, 52, -6), LatPar (-50, -56, 28; 44, -64, 38), HF (-24, -20, -24; 24, -22, -24), IPS (-14, -80, 44; 12, -82, 40), FEF (-30, 4, 54; 26, -2, 54), and MT+ (-58, -52, -2; 54, -66, 2). All of these regions were used where possible. For the analyses of temporal resolution and spatial resolution, where partial brain coverage became an issue, only the pC,

LatPar, HF, IPS, Mot, and Aud ROIs were tested. Note that the slice positioning for dataset 3 was intentionally selected so that these critical regions would be sampled even for the condition that afforded only partial brain coverage.

Signal variation due to respiration

Dataset 6 was explicitly designed to identify resting respiratory neural activity associated with the BOLD signal (Evans et al. 2009) and was used here to investigate the influence of respiration on fcMRI analysis and whether the preprocessing steps adequately removed influences of respiration. That is, it may be possible to remove unwanted contributions of respiration by regressing out nuisance signals that indirectly track respiration (e.g., ventricular, whole-brain).

Respiration (airway flow) was measured during fMRI data acquisition with a simple breathing apparatus consisting of a pneumotach (MLT300L, ADInstruments, Colorado Springs, CO) connected via y-piece to comfortably fitting tubing in each nostril (Nasal Puffs, Cpap Pro, Simi Valley, CA). Tidal volume was calculated by integrating airway flow. Respiration volume per time (RVT) was computed as a measure of variation in respiration similar to Birn et al. (2006). First, the envelope of breath-to-breath variability was computed by connecting the maximum inspirations and, separately, connecting the maximum expirations. Second, the period of respiration was calculated for each time point in the fMRI time series as the distance between the two closest maximum inspirations. Finally, RVT was computed for each time point by taking the difference between maximum inspiration and maximum expiration divided by the period of respiration (Birn et al. 2006).

To analyze the influence of respiration on fcMRI, we computed correlation maps showing signal variation due to respiration as follows. First, RVT was correlated with the signal from each acquired voxel during the BOLD run. To take into account the likely possibility of a delay between respiration and its influence on the BOLD signal, the correlation procedure was repeated for 21 shifts of RVT (from −10 to +10 s in 0.5-s increments). Then for each voxel, the largest positive and negative correlation between RVT and BOLD signal was chosen from those 21 shifts to obtain a map of positive and negative correlations between RVT and BOLD signal before and after preprocessing, to both visualize the respiration signal in the raw data and determine whether it remains following preprocessing.

To investigate whether regression of RVT might change functional connectivity measures, correlation maps with the pC seed region were calculated following completion of all of the preprocessing steps with and without additional removal of RVT. The time-shifted maximal positive and negative RVT contribution was regressed from each acquired voxel after full preprocessing, and the residual time course from each voxel was correlated with the time course from the pC seed region. In this manner, we could conservatively assess the additional benefit of direct removal of respiration above that of indirect removal via preprocessing.

Independent component analysis (ICA)

Probabilistic independent component analysis (pICA) was implemented using MELODIC software (Beckmann and Smith 2004). Data first underwent standard preprocessing as described in the preceding text up to (and including) the application of a Gaussian spatial smooth of 6 mm FWHM. For each subject, the first functional run was then fed into the MELODIC software and also separately further processed and analyzed using our standard seed-based approach. The pICA procedure was set to estimate per subject the optimal number of independent components (Minka 2000) that averaged 54 ± 4 (SD) components (range: 47–64). For each component, a z-score at every voxel was computed, reflecting the degree to which the time series of that voxel is associated with the time series of the specific component.

An automated template matching procedure as described by Greicius et al. (2004) was used to select the component that best fit a binary template of the motor network from the resulting probability maps. The template was created by selecting all voxels with a correlation value >0.12 from a correlation map of the motor cortex seed region from the same dataset using the coordinates from Fig. 2. The template-matching procedure involved taking the average z score of all voxels within the template minus the average z score of all voxels outside the template and selecting the component in which this difference (the goodness of fit) was the greatest. The best-fitting z maps for the motor network of all 48 subjects were then averaged and plotted on the average anatomical scan. The same template matching procedure was used to select the best fitting components for the visual, default, and attention networks.

Bartlett correction factor

Because individual time points in the BOLD signal are not statistically independent, the degrees of freedom used in determining significance of a correlation value in an individual subject must be corrected. Misestimating significance due to correlation across time points becomes particularly problematic for short run lengths (where degrees of freedom are low) and at short acquisition repetition times (TR; where autocorrelation between time points is increased). To correct for the temporal correlation structure, we used Bartlett's theorem to adjust the effective degrees of freedom (Jenkins and Watts 1968). The Bartlett correction factor (BCF) was applied when statistical significance was dependent on temporal degrees of freedom as is the case in our calculation of power to detect correlations with varying run length (dataset 3b). The BCF is not necessary when performing second-level random effects tests on group data, where degrees of freedom is determined by the number of subjects. The BCF for dataset 3b, computed as the integral across time of the square of the autocorrelation function, was 1.62. The t-value corresponding to the correlation value for each network for each subject was calculated as: $t(n − 2/BCF) = r * sqrt\{[(n − 2)/BCF]/(1 − r^2)\}$. As one illustration of the influence of run length, the significance of t-values averaged across subjects and after $−log(p)$ transformation were plotted for each network at each scan length (Fig. 11*C*).

Effect of task on functional connectivity

To explore the influence of the task on fcMRI analysis, datasets 3–5 systematically varied the task across functional runs. For all other datasets, participants fixated on a cross-hair (plus sign) for the entire duration of the functional run and were asked to stay awake and remain as still as possible.

Datasets 3 and 4 directly contrasted visual fixation (fix) with an eyes-closed rest (ECR) task condition. During the ECR task, participants kept their eyes closed while resting and were asked to stay awake and remain as still as possible. As the results will reveal, correlations are attenuated in the networks tested during ECR as contrasted with fix. To further explore the task effects, dataset 5 again repeated the fix and ECR conditions and added two additional task conditions: eyes open rest (EOR) and continuous semantic classification (class). For the EOR task, subjects were asked to keep their eyes open during the entire duration of the scan, no visual fixation cross-hair was present, and the screen was turned off. This condition is particularly important because it allows exploration of whether something as simple as asking participants to open their eyes can recover signal lost in the ECR condition (without having to set up a visual projection system). For the class task, participants decided whether centrally presented visual words represented abstract or concrete entities—a moderately demanding task that engages external attention and controlled processing (Demb et al. 1995; Wagner et al. 1998; see Buckner et al. 2009). Participants were instructed to respond quickly and accurately with a right-hand key press. The task was self-paced with a new word appearing 1,000 ms after the response, hence minimizing downtime between trials and the potential for mind wandering (Antrobus 1968; Antrobus et al. 1966; D'Esposito et al. 1997). The mean response time was 1,024 ± 275 ms and mean accuracy was 91 ± 10%. In all studies where the task varied across runs, the order of task condition was counterbalanced across subjects.

RESULTS

Preprocessing reduces nonspecific correlation among brain regions

We first explored the influence of preprocessing steps on correlation strengths within well-studied networks. Mean correlation strengths within and between default, attention, and reference networks were quantified after each of the preprocessing steps that are commonly applied to fcMRI data. After preprocessing, the correlation values among default network regions as well as among attention network regions are expected to be positive, correlations between default and attention networks are expected to be negative, and correlations between reference regions are expected to be zero. The results showed that the relative correlation strengths are largely preserved across processing steps while differences between networks are enhanced with subsequent steps, and correlations among reference regions approached zero (Fig. 3).

After all preprocessing steps were carried out, the average correlation strength in z-values for default, attention, and ref-
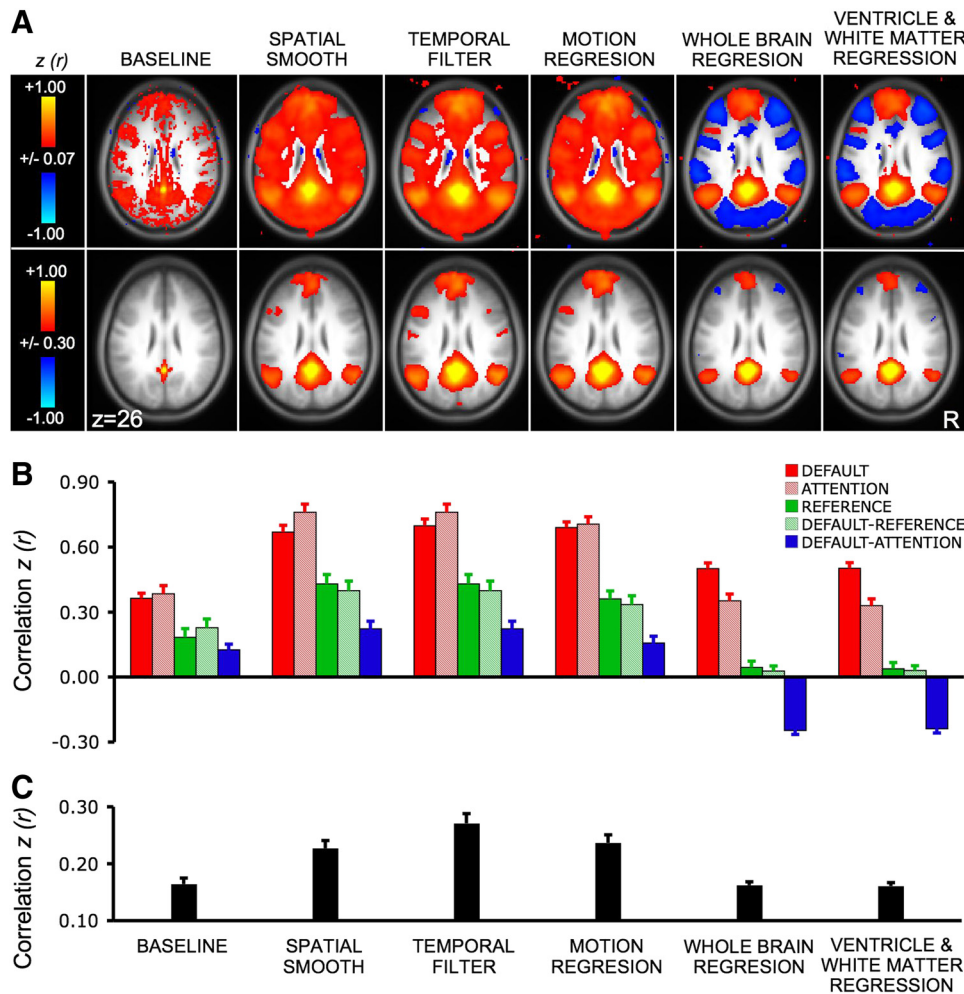
FIG. 3. The influence of preprocessing steps on correlation estimates. Prior to fc-MRI analysis, data undergo a series of preprocessing steps. The influences of preprocessing steps on both positive and negative correlations are illustrated. *A*: fcMRI maps with the posterior cingulate (pC) used as a seed region are shown for the sample of 48 subjects from dataset 1 at two different thresholds. Each map illustrates the effect of an additional preprocessing step (e.g., baseline includes no preprocessing; spatial smooth includes only the spatial smooth; temporal filter includes both spatial smoothing and the low-pass temporal filter). Note that robust negative correlations (also called "anticorrelations") emerge following whole-brain regression. *B*: mean correlation strength within and between the default, attention, and reference networks are quantified. Note that the relative correlation strengths are largely preserved across processing steps. Differences between networks enhance with subsequent steps and the correlation in the reference network approches zero when whole-brain (global) regression is implemented. *C*: an estimate of spurious correlations/noise is plotted. Noise is here defined as the absolute mean value of correlations with the pC seed region in selected brain regions that typically reveal minimal correlation with the pC seed region.

erence regions were 0.50 ± 0.03, 0.33 ± 0.03, and 0.04 ± 0.03 (mean $\pm$ SE), respectively. Mean correlation strength between default and attention networks was -0.24 ± 0.02. Estimates of noise in correlation maps reduced with motion and whole-brain regression (Fig. 3*C*). Thus preprocessing steps have the desired effect of increasing contrast between network correlations and reducing nonspecific/noise correlations.

However, it should also be noted that the correlations within networks were present even when minimal preprocessing steps were applied (e.g., only a spatial smooth). When the threshold was raised above the level of nonspecific correlations, the topography of the default network was nearly identical between preprocessing involving only spatial smoothing and full preprocessing (Fig. 3*A*). This important detail implies fcMRI analysis is robust and, when sufficient data are averaged, positive correlation patterns persist across processing variations. However, the magnitude of the correlation is influenced by processing choices.

Robust "anticorrelations" between networks were only found after preprocessing

A controversial issue has arisen regarding how to interpret negative correlations, sometimes referred to as anticorrelations, in fcMRI data that have been processed using whole-brain (global) signal normalization (Chang and Glover 2009b; Fox et

al. 2009; Murphy et al. 2009). The reason for the controversy is that whole-brain normalization shifts the correlation distribution to have a mean near zero thereby guaranteeing negative correlations even if no such correlations are initially present in the data (e.g., see Murphy et al. 2009 for discussion). Anticorrelations in our data emerged after whole-brain regression including the prototypical strong negative relationship between the attention and default networks (Fox et al. 2005; Fransson 2005). The negative correlations were present after (-0.24 ± 0.02) but not prior to whole-brain regression (0.16 ± 0.03; Fig. 3, *A* and *B*). Examination of the group correlation images revealed no detectable negative correlations in cortical regions prior to whole-brain regression even when a liberal statistical threshold is applied (Fig. 3*A*) (but see Chang and Glover 2009b for a different result). Prior to whole-brain regression, the correlation maps were dominated by nonspecific positive correlations throughout the brain. These results illustrate both why signal regression is performed in typical analyses and also why negative correlations must be cautiously interpreted.

Preprocessing minimizes the influence of respiration on network correlations

A specific challenge of fcMRI analysis surrounds confounding influences of physiological noise, in particular slow fluctuations induced by respiration that have frequency compo-

nents overlapping those related to fcMRI signals. Here we tested directly whether typically applied preprocessing steps effectively minimize the confounding influence of respiration. First, we mapped the correlation pattern associated with respiration using dataset 6 (Fig. 4*A*). Results revealed strong respiration-correlated signals especially along the midline and brain edges. Critically, these correlations were minimized following application of the preprocessing steps (Fig. 4*B*). Next correlation maps with the pC seed region were calculated following preprocessing without and with additional removal of respiration variation (Fig. 4, *C* and *D,* respectively). After preprocessing, the additional removal of respiration-correlated signals minimally influenced the results, suggesting that preprocessing that removes signals associated with nonspecific signal sources through regression is sufficient to minimize the confounding influences of respiration.

Seed-based and ICA techniques yield similar networks

To ensure that our results are likely to generalize to multiple analytic methods, dataset 1 was analyzed with both seed-based analysis (Biswal et al. 1995; Vincent et al. 2006) and pICA as implemented by MELODIC software (Beckmann and Smith 2004). Highly similar networks for motor, visual, default, and attention networks were revealed with both analysis techniques (Fig. 5). Similarities between the seed-based and ICA measures

of the default network were also evidenced by a significant relation between correlation of default network seed regions and the goodness of fit of the default component obtained with ICA ($r = 0.45$, $P < 0.01$; Fig. 6). Thus while seed-based and ICA approaches have distinct strengths and can yield different results, for the main networks tested here, they both extract similar signal components.

Functional connectivity strength and the topography of correlation maps are reliable

We conducted multiple analyses to estimate the reliability of fcMRI and also to estimate the duration of MRI acquisition time required to obtain reliable results. In our first analysis, functional connectivity estimates for the default, attention, and reference networks from dataset 2 were calculated for each of six subjects across two sessions with a mean delay of 7.7 ± 5.5 (SD) days. The sample size was not sufficient to estimate within-network reliability but provided an opportunity to estimate reliability that included between-network variance. This dataset was particularly valuable because of the large amount of rest data available for each session. Results showed high reliability ($r = 0.85$, $P < 0.001$) across sessions when all data were analyzed (8 functional runs per session; 41 min 20 s worth of data). Surprisingly, the reliability was still moderate to high ($r = 0.71$, $P < 0.01$) when only a single run of
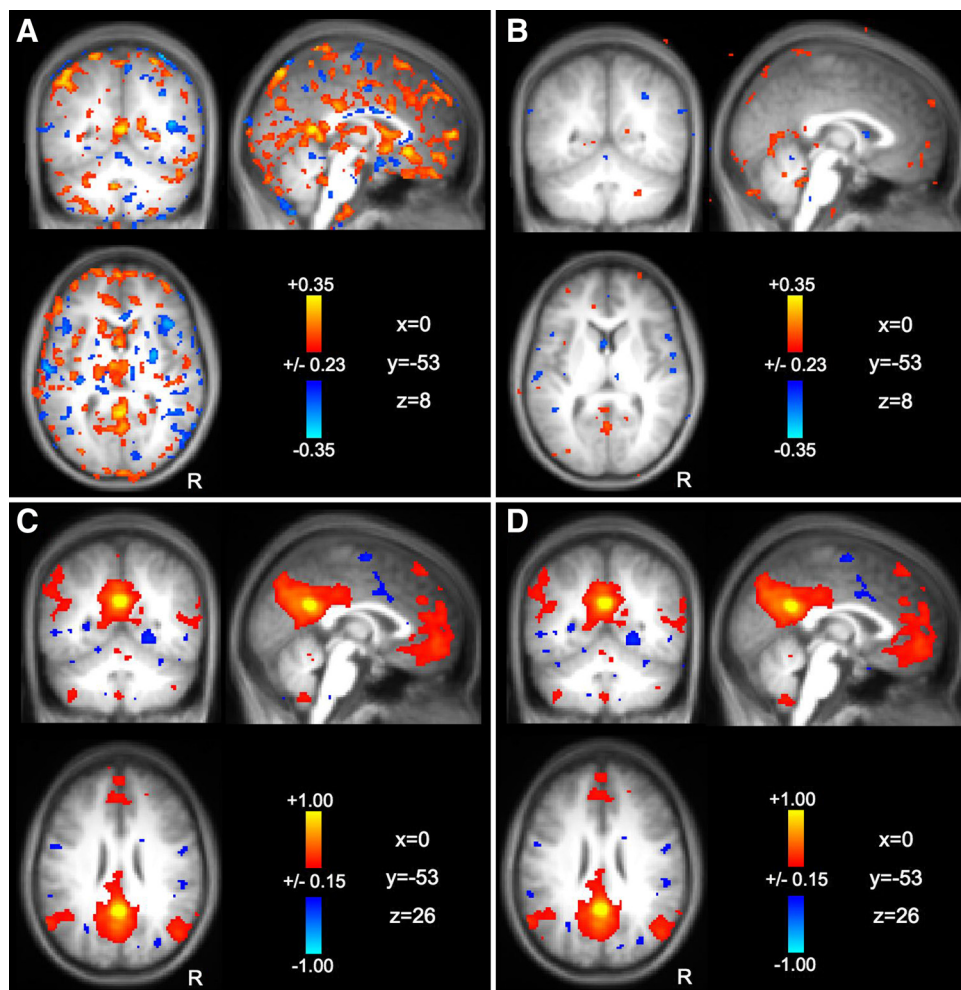

FIG. 4. Appropriate data preprocessing minimizes the effect of respiration on functional connectivity. Correlation maps with signal variation due to respiration from dataset 6 are shown before (*A*) and after (*B*) application of the full sequence of fcMRI preprocessing steps that are illustrated in Fig. 3 (the data for *A* underwent preprocessing up to and including Gaussian smoothing). Note that the respiration signal correlations are present in the raw data and also that they are largely removed by preprocessing. Correlation maps with the pC seed region are shown following preprocessing without (*C*) and with (*D*) additional removal of respiration variation. Note that after preprocessing, the additional removal of respiration-correlated signals minimally influences the results. These combined observations suggest that respiration influences the data but the effect can be effectively minimized by appropriate data preprocessing.
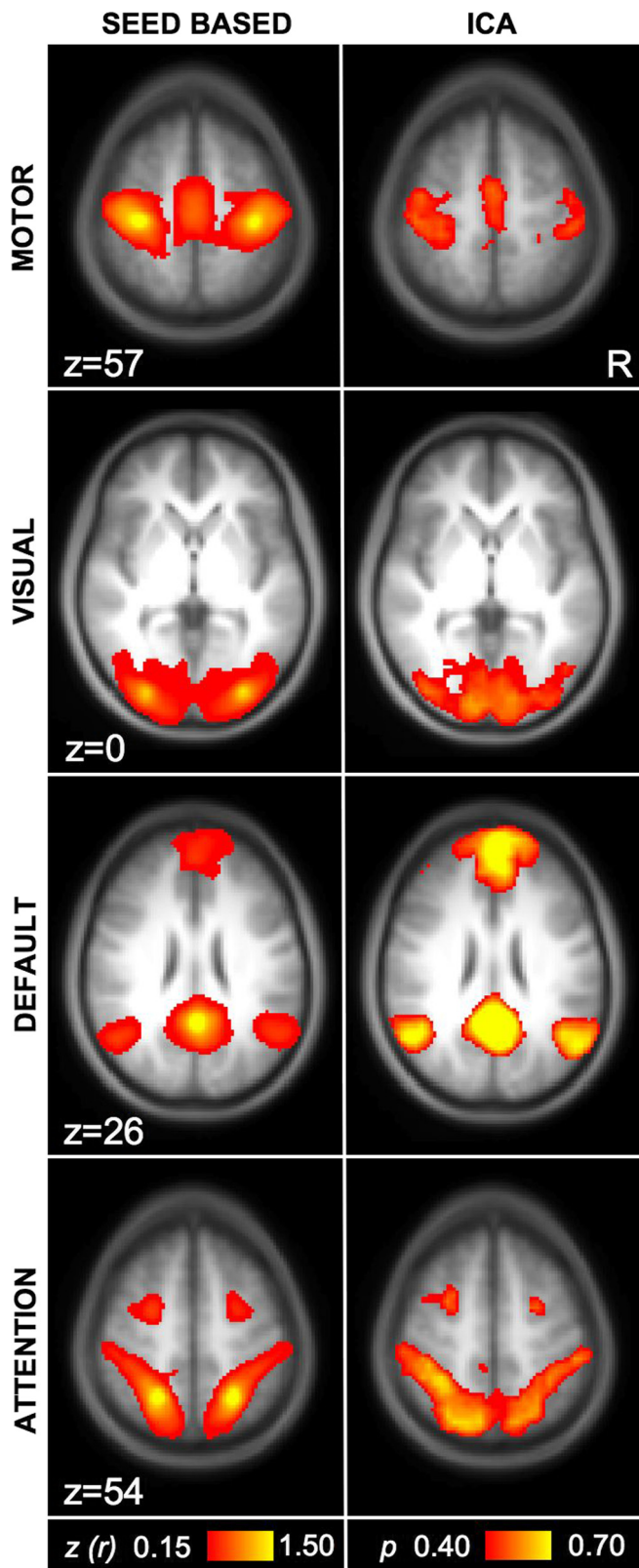
FIG. 5. Similar functional connectivity results are obtained by seed-based and independent component analysis (ICA) techniques. *Left*: images were obtained using seed-based fcMRI for regions within motor, visual, default, and attention networks (computed with Mot, Vis, pC, and IPS seed regions from Fig. 2). *Right*: images were obtained from the same data using ICA as implemented by MELODIC software (Beckmann and Smith 2004). Note that the 2 approaches, for the networks analyzed in this paper, yield convergent results.
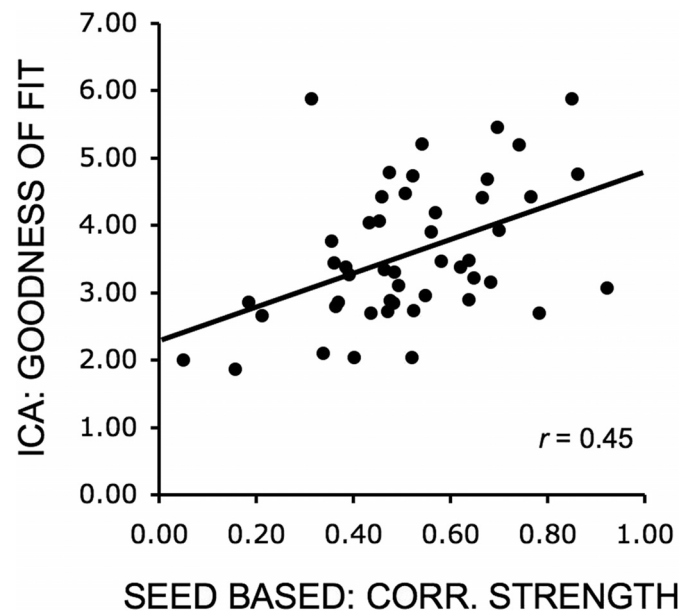
FIG. 6. Similarities between seed-based and ICA measures of the default network. Mean correlation among default network regions as measured by the seed-based approach was significantly correlated with the goodness of fit of the default component obtained by ICA.

data was considered (total of 5 min and 10-s rest data per session; Fig. 7).

Motivated by the possibility that a single run is sufficient to obtain reliable correlation estimates, we explored reliability for each network separately for dataset 1 that included 48 subjects. Six minutes of rest data were employed for each estimate. Quantitative estimates were compared between independently processed runs with run order counterbalanced. Results revealed moderate to high correlations for the default and attention networks ($r = 0.63$, $P < 0.001$ and $r = 0.67$, $P < 0.001$, respectively), and low correlation for the reference regions ($r = 0.19$, $P = 0.18$; Fig. 8).

In a third analysis, we explored reliability across sessions for dataset 2 by examining the overlap of functional connectivity maps of the pC seed region for both eight runs and one run per subject (Fig. 9, *A* and *B,* respectively). Percent overlap across sessions in the 3D volume was calculated by dividing the number of voxels that were above threshold in both sessions (session 1 ∩ session 2; depicted in the bottom row of Fig. 9, *A* and *B,* as yellow) by the number of voxels above threshold for either session (session 1 ∪ session 2; depicted in Fig. 9, *A* and *B, bottom,* as red+yellow+blue) multiplied by 100. The average percent overlap across sessions was 65% for eight runs (range: 57–78) and 45% for one run (range: 23–38). Variability of pC seed correlation maps across participants is depicted in the overlap image in Fig. 9, *A* and *B, far right*. The average percent overlap of the pC correlation map for any two individual subjects from session 1 was 88% (for session 2: 79%) for eight runs and 77% (76%) for one run. These estimates of overlap can be taken as guidelines only and will be dependent on the threshold value (although our threshold was chosen without reference to the quantitative overlap produced). Note that both the map estimate and reliability improve when more data are averaged per subject but again that a single functional run is sufficient to produce surprisingly reliable results across subjects and sessions (Fig. 9*B*). We will return quantitatively to

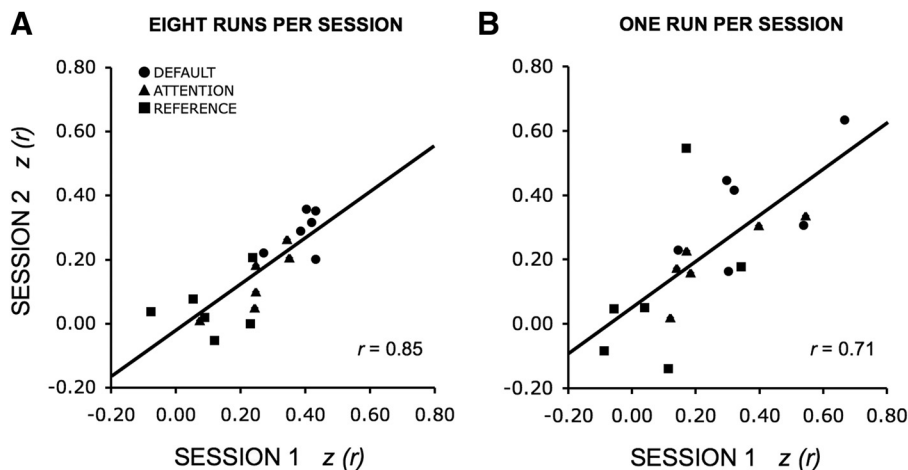**A**   **EIGHT RUNS PER SESSION**   **B**   **ONE RUN PER SESSION**

FIG. 7. Quantitative estimates of functional connectivity strengths are reliable across sessions on separate days. Functional connectivity estimates for the default, attention, and reference networks from dataset 2 are plotted for each of 6 subjects across 2 days. Each point represents the mean correlation strength within 1 network for 1 subject. Reliability across sessions was high with correlations of 0.85 (*A*) when 8 functional runs were analyzed per subject (total of 41-min and 20-s rest data per session). and 0.71 (*B*) when only a single functional run was analyzed per subject (total of 5-min and 10-s rest data per session). Note that longer acquisitions did improve reliability, however, surprisingly reliable estimates were obtained with only ~5 min of data per subject.

the question of how much data are needed to make stable estimates of functional connectivity in the following text.

In a final analysis, functional connectivity maps for motor, visual, default, and attention networks were examined across four distinct subject groups that were constructed by randomly dividing the 48 subjects from dataset 1 into four independent groups of 12 subjects. As might be expected from the preceding results, the maps were highly similar across the four independent datasets (Fig. 10). Percent overlap of the map of the motor network for any pair of datasets was 97% on average, 87% for visual, 90% for default, and 98% for attention. These analyses emphasize that there are sufficient central tendencies across subjects such that group averages provide highly similar fcMRI map estimates from one dataset to the next.

Functional connectivity strengths can be estimated from rapid data acquisitions

To further explore the effect of acquisition duration on functional connectivity estimates, we performed fcMRI analysis on incremental durations of scan times ranging from 2 to 12 min for the six participants in dataset 3. Average correlation strengths within and between default, attention, and reference networks stabilized after using ~5 min of data (Fig. 11*A*). These estimates show that multiple distinct correlation strengths can be obtained in as little as 4–5 min. In addition, estimates of spurious correlations decreased in approximate proportion to the square root of the sampling time (Fig. 11*B*) and approach asymptotic levels within 5–6 min. We also calculated the *t*-value of the individual subjects' correlation values with degrees of freedom that were corrected using the Bartlett correction factor (see METH-ODS for details). The corresponding *P* values show that the ability to detect significant correlations within different networks in individual subjects increases with increasing run length (Fig. 11*C*) but, again, relatively short data-acquisition epochs are surprisingly powerful.

Estimates of the correlation strengths for the default, attention, and reference networks were computed for 4-min data epochs for the beginning, middle, and final portions of the 12-min run (Fig. 12). Estimates were stable establishing that the 4-min run lengths were sufficient to estimate connectivity reliably and also that position within the run had minimal effect on the estimate. That is, the estimates were stationary across

the 12 min. The largest difference was found from middle (0.39 ± 0.05) to late (0.55 ± 0.12) for the default network, which was not significant [*t*(5) = 1.85, *P* = 0.12].

Functional connectivity strength depends minimally on run structure, temporal resolution, and spatial resolution

The remaining results focus on experimental manipulations that were conducted to probe optimal acquisition procedures. Analysis of dataset 3 revealed that differences in run structure (either a single 12-min run, or 2 6-min runs), temporal resolution (2.5 or 5.0 s TR), and spatial resolution (2 vs. 3 mm isotropic voxels) had minimal effect on functional connectivity strengths (Fig. 13). The largest difference was found for temporal resolution (correlation between the default and attention network) where group averages for a 2.5- and 5.0-s TR were −0.28 ± 0.07 and −0.33 ± 0.07, respectively, which was not significant [*t*(5) = 0.98, *P* = 0.37].

Functional connectivity strength is influenced by task

fcMRI data have been collected during varied rest and task states. In a series of three studies, we explored differences in functional connectivity strengths for BOLD runs during which participants performed different tasks. Run order was counterbalanced. The only difference across conditions was the tasks performed by the participant. Results are presented in Fig. 14. For dataset 3, participants fixated on a cross-hair (fix) or rested with their eyes closed (ECR). A repeated-measures ANOVA with task (fix and ECR) and network (default and attention) revealed a trend for stronger correlations for fix than for ECR [*F*(5,1) = 6.00, *P* = 0.06]. The trend was sufficient to motivate collection of a second dataset with the same conditions (dataset 4). The effect of stronger correlations for fix than for ECR was significant [*F*(11,1) = 15.94, *P* < 0.01].

Because fixation and eyes closed rest potentially differ on both dimensions of arousal and level of control (fixation being a more controlled task), we replicated and extended the analysis of task conditions to also include an eyes open rest (EOR) condition and a continuous semantic classification task (class) in a third study (dataset 5). A repeated-measures ANOVA with four tasks (fix, EOR, ECR, and class) and two networks (default and attention) revealed a significant main effect of task [*F*(13,3) = 5.15, *P* < 0.05]. As before, ECR showed numer-

A   DEFAULT
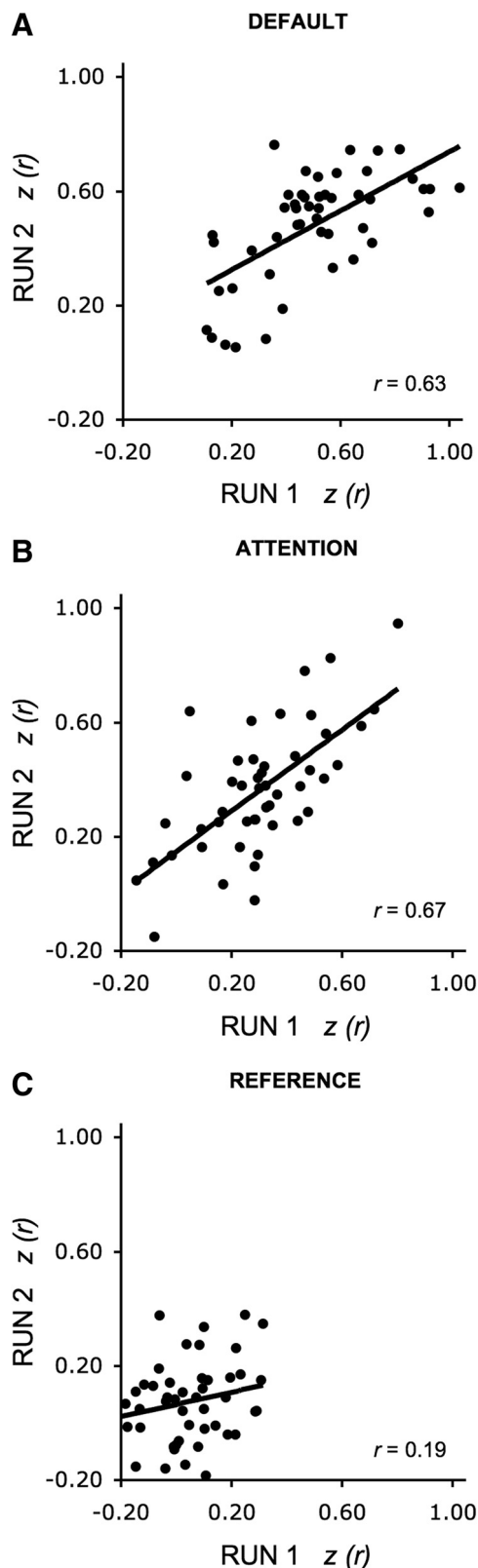

B   ATTENTION

C   REFERENCE

FIG. 8. Quantitative estimates of functional connectivity strength are reliable across 2 BOLD runs from a single scan session. Reliability of measures of the default, attention, and reference network was explored across 2 BOLD runs from a single scan session (dataset 1). Six minutes of rest data were used for each run and independently processed with run order counterbalanced. Each point represents a unique subject. Moderately high test-retest reliably was obtained for the default and attention networks. Lower, nonsignificant correlation was obtained for the reference network.

ically lower correlations than fix in an ANOVA of two tasks (fix and ECR) and two networks [default and attention; $F(15,1) = 3.03$, $P = 0.10$]. However, an ANOVA of two tasks (fix and EOR) and two networks (default and attention) revealed no significant effect of task [$F(15,1) = 0.46$, $P = 0.51$], which indicates that the loss of correlation in the ECR condition could be fully recovered by simply having the subjects rest with their eyes open. Correlations were significantly lower for class when compared with fix [$F(15,1) = 11.14$, $P = 0.004$] and EOR [$F(15,1) = 13.17$, $P = 0.002$], and numerically lower for class when compared with ECR [$F(15,1) = 2.9$, $P = 0.11$].

In sum, functional connectivity strength within the default and attention networks were significantly diminished for ECR when compared with fix. Consistent with recent results of C. Yan et al. (2009), having the subjects open their eyes mitigated this effect suggesting that instructing subjects simply to keep their eyes open is a practical condition to use in studies where setting up a display is difficult. Having the participants engage a continuous self-paced classification task resulted in the weakest correlations in the networks examined and is a reminder that fcMRI estimates are influenced by present processing demands in addition to anatomic connectivity.

DISCUSSION

fcMRI offers a promising tool for characterizing the connectivity of human brain systems and variations between individuals. The introduction framed the importance of fcMRI to human neuroscience as well as described current practices in the application of the approach. The results from six empirical studies were presented next in order to characterize properties of commonly used fcMRI preprocessing procedures, the reliability of fcMRI data, and the influences of different acquisition parameters and task states. Here we summarize the primary observations and provide practical recommendations for fcMRI methods and analysis. We conclude by discussing possible future directions. The main findings can be summarized as follows.

First, fcMRI detects correlations that are constrained by connectional anatomy and thus can be used to provide insight into the connectional architecture of the human brain. However, fcMRI does not solely reflect direct anatomic connectivity. Functional connectivity patterns are affected by task states and correlations extend across circuits that are connected through polysynaptic projections and common inputs. These considerations place constraints on the utility of fcMRI while also providing opportunities. For example, fcMRI is particularly useful for examining the architecture of large-scale polysynaptic brain systems.

Second, typical preprocessing procedures used for fcMRI analysis result in robust estimates of connectivity within brain systems and reduce nonspecific (noise) correlations. Critically, regression of nuisance correlations that can be estimated from the data (via white-matter, ventricular, and whole-brain signals) are sufficient to reduce artifacts associated with respiration and other sources of spurious noise. Certain applications may require the direct measurement of cardiac and respiratory noise (e.g., Chang and Glover 2009b).

Third, preprocessing that includes whole-brain (global) signal normalization shifts the distribution of correlations. Robust negative correlations (anticorrelations) between net-
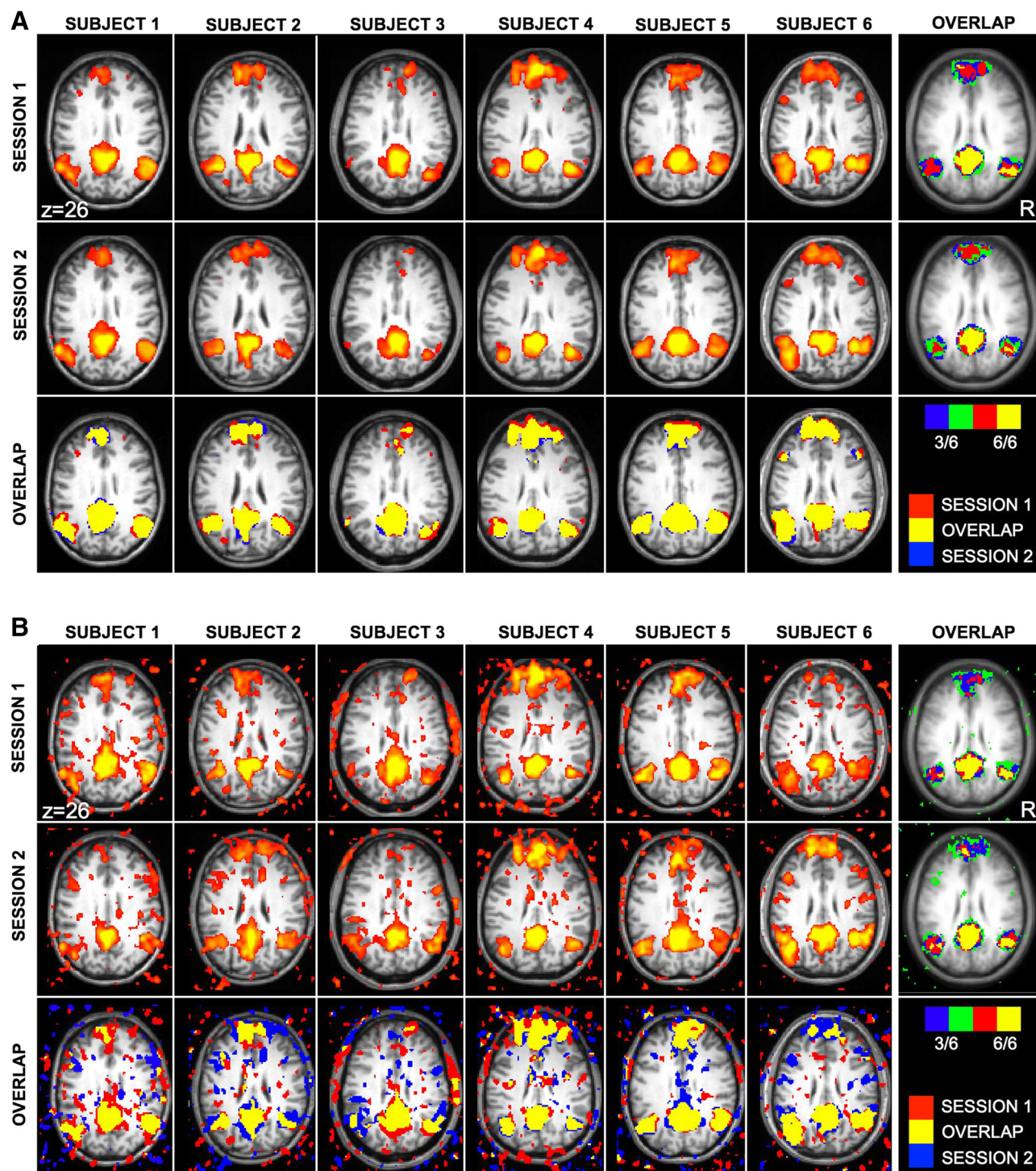
FIG. 9. Functional connectivity networks are reliable across data sessions and between individual subjects. Reliability of functional connectivity maps for pC is depicted in the overlap image for 8 runs per subject (*A*) and 1 run per subject (*B*). Data are the same as Fig. 7. Variability of pC seed correlation maps across participants is depicted in the overlap image in the *far right* of both *A* and *B*. Maps of individual subjects were thresholded at $z(r) > 0.25$. Note that the map estimate and reliability improve with data averaging but also that a single functional run of ~5 min is sufficient to produce results that are reliable across sessions and reproducible between subjects.

works are present after normalization but not before. While this result does not itself mean that all forms of negative correlation are artifacts of processing procedures, it does indicate that whole-brain signal regression can induce shifts in the sign of correlations that should be carefully considered before they are functionally interpreted.

Fourth, seed-based methods and ICA yield similar results, indicating that these complementary methods extract common signals (see also Beckmann et al. 2005; Long et al. 2008). Of relevance, the properties and recommendations for optimization will likely generalize to both forms of functional connectivity data analysis.
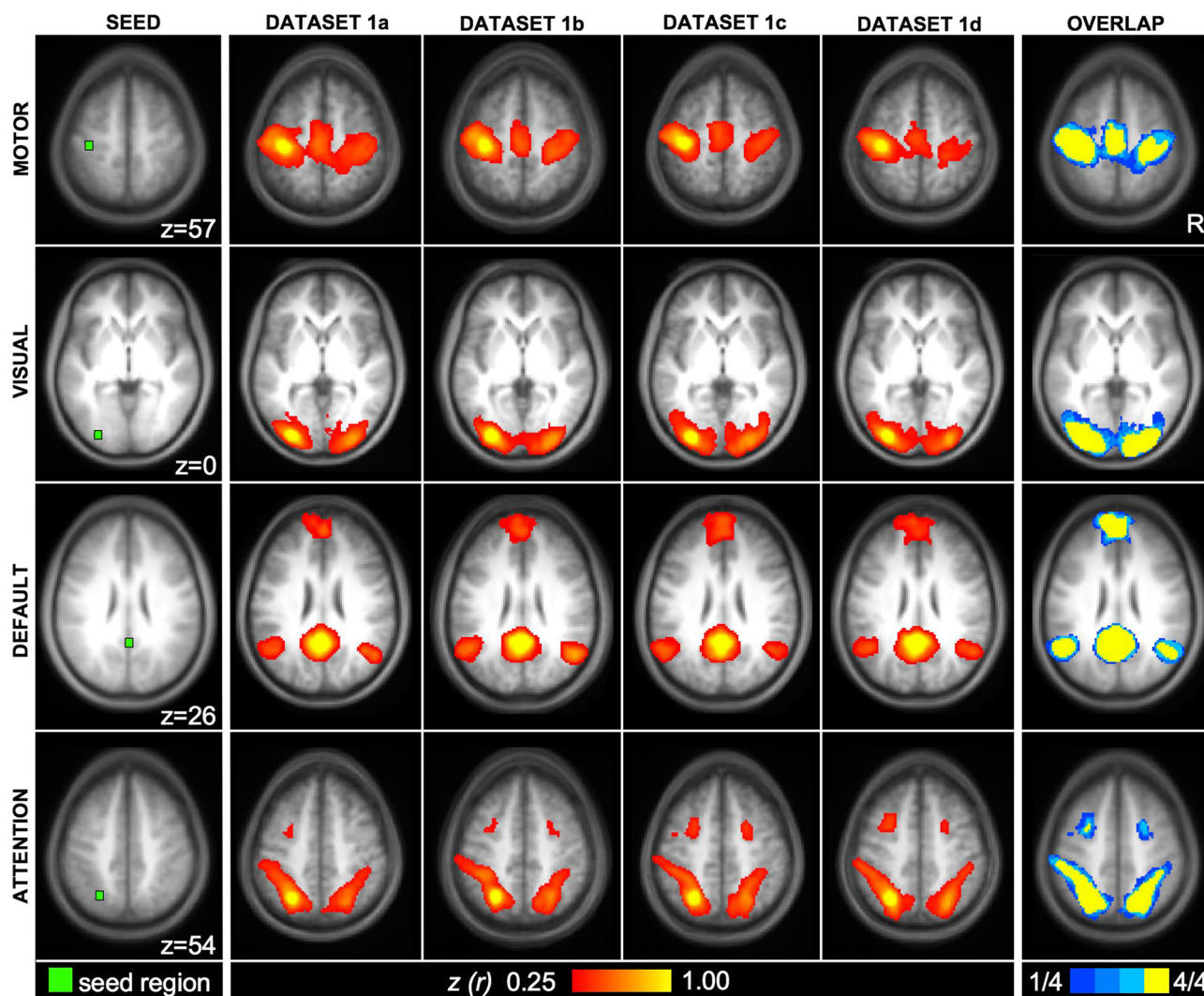
FIG. 10. Functional connectivity networks are reliable across independent subject groups. Functional connectivity maps for motor, visual, default, and attention networks were highly similar across 4 independent datasets. *Far right*: overlap across different datasets; voxels common across all 4 groups are colored yellow. Each dataset combines 12 participants from dataset 1. Seed regions were the same as given in Fig. 2.

Fifth, functional connectivity strength and the topography of correlation maps are reliable across subjects and sessions and are replicable across independent subject groups. Our reliability estimates fell within the moderate range. Thus fcMRI measures may be appropriate phenotypes for exploring individual and group differences. Nonetheless, power calculations should be careful to consider that reliability estimates fell in the moderate range for relatively strong network correlations; reliability estimates will be less for weaker correlations.

Sixth, functional connectivity strength can be estimated rapidly and, with the functional resolution explored here, depends minimally on temporal and spatial resolution. Specifically, estimates of the connectivity strength of commonly studied networks (i.e., the default network and the dorsal attention system) benefited minimally by extending the data acquisition beyond 6 min. Thus while increasing acquisition time does reduce noise, the signal strength of fcMRI is sufficient to allow efficient, brief whole-brain imaging protocols.

Seventh, many forms of task condition yield highly robust fcMRI estimates including rest and continuous task conditions. Nonetheless, functional connectivity strength is influenced by task such that fixation and eyes open rest yielded stronger correlations in the networks examined than eyes closed rest or a continuous semantic classification task. The surprising finding that simply opening one's eyes, even with unconstrained eye movements, is sufficient to return the power and stability of the fcMRI estimates to a level comparable to fixation presents a practical option for studies where stimulus display is not available.

Preprocessing, physiological noise, and anticorrelations

Correlations within the default network and the dorsal attention system were readily observed with only minimal preprocessing steps and remained after full preprocessing. Preprocessing confers noticeable benefits to fcMRI data analysis. Spurious correlations between reference regions from the visual, auditory, and motor corticies were present before preprocessing but approached zero after preprocessing. Thus appropriate preprocessing appears to reduce nonspecific correlations while leaving true correlations intact.

A specific concern regarding the validity of fcMRI measures is the potential for confounding influences of physiological
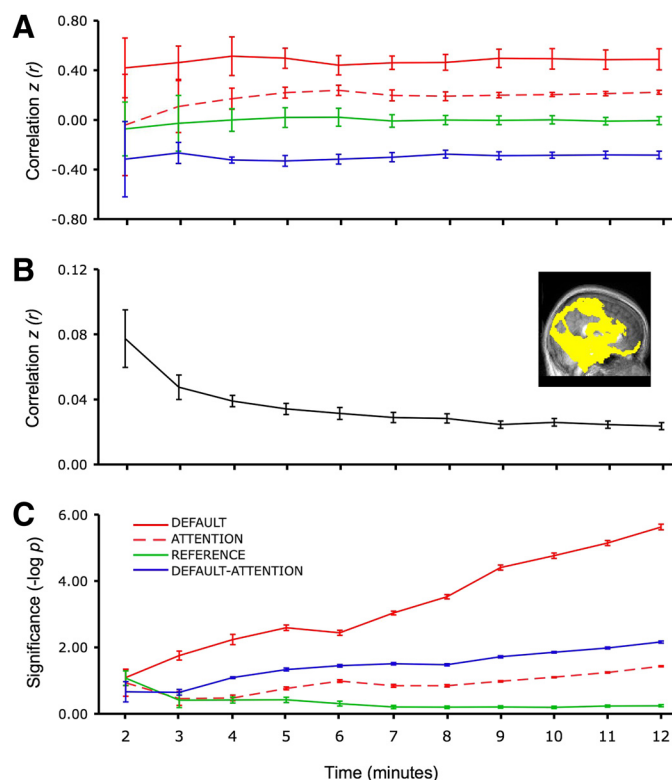
FIG. 11. Functional connectivity networks can be assessed using brief acquisition times. Functional connectivity analysis was performed for incremental durations of scan times ranging from 2 to 12 min for 6 subjects. *A*: correlation strengths within and between default, attention, and reference networks. Estimates of correlation strengths stabilize rapidly. *B*: noise, defined as spurious correlations in selected regions (the inserted image depicts the mask of these regions), decreases with increasing acquisition time. *C*: the mean within-subject significance probability is plotted for each network to show the ability to detect significant correlations. *P* values are estimated using a model that computes effective degrees of freedom taking into account the temporal correlation of the time series (see text). Error bars represent SE.

noise, in particular slow fluctuations associated with respiration (Birn et al. 2006, 2008b). We found that variations in respiration had a significant effect on the BOLD signal when minimal preprocessing was applied but that typical preprocessing steps effectively minimized the influence of respiration on network correlations. Specifically, after preprocessing, correlation maps of the default network were almost identical before and after additional removal of variations in respiration (Fig. 4). This result parallels findings from Birn and colleagues (2006), who showed that default network maps were qualitatively similar before and after removal of variations in respiration (compare their Fig. 7, *C* and *D*).

Moreover, it was recently shown that sophisticated statistical correction of both respiratory and heart rate variation resulted in only minor changes in correlations among default network regions ($z(r)$ from 0.57 to 0.53) (Van Buuren et al. 2009). Others have shown that in addition to removal of noise, physiological correction can increase signal correlations (Chang and Glover 2009b). Measurement of physiological noise provides a unique opportunity for those who are interested in the effect of respiration and/or heart rate on the BOLD signal and allows the direct removal of physiological signal variation. However, from a practical perspective, typical preprocessing that removes signals associated with nonspecific signal

sources, such as whole-brain, ventricle, and white matter regression, appears sufficient to minimize confounding influences of physiological noise.

Another controversial issue surrounds the interpretation of negative correlations (anticorrelations) in fcMRI data that have been processed using whole-brain signal normalization. Whole-brain signal normalization shifts the correlation distribution to have a mean near zero, thereby either producing negative correlations (even if no such correlations are initially present in the data) or artificially magnifying true negative correlations (e.g., see Chang and Glover et al. 2009b; Fox et al. 2009; Murphy et al. 2009; Vincent et al. 2006; for discussion). Our results are consistent with the observation that robust anticorrelations are present following regression of the whole-brain signal but not before and therefore that such negative correlations do not unambiguously imply that brain systems are in functional competition with one another (Fox et al. 2005; Fransson 2005). Thus the present results reinforce the notion that negative correlations after whole-brain signal regression should be interpreted with the utmost caution (Murphy et al. 2009; Weissenbacher et al. 2009). Future studies that use alternatives to whole-brain signal regression (see e.g., Chang and Glover 2009b; Fox et al. 2009) or other approaches to measure large-scale neuronal interactions (such as available in humans with surgically implanted subdural electrodes or animal models) may provide converging evidence on the question of whether negative correlations warrant neurophysiological interpretation.

Practical considerations for the robust application of fcMRI

The combined results offer a number of practical recommendations for the application of fcMRI.

LENGTH OF ACQUISITION. A promising property of fcMRI data is that individual-subject and group-level functional connectivity strengths can be estimated with rapid data acquisitions. As noted in the preceding text, estimates of correlation strengths stabilize by 5–6 min of data acquisition for well-studied brain systems. Figures 7–9 illustrate that individual-subject maps are stable with 5-min data acquisitions. Increas-
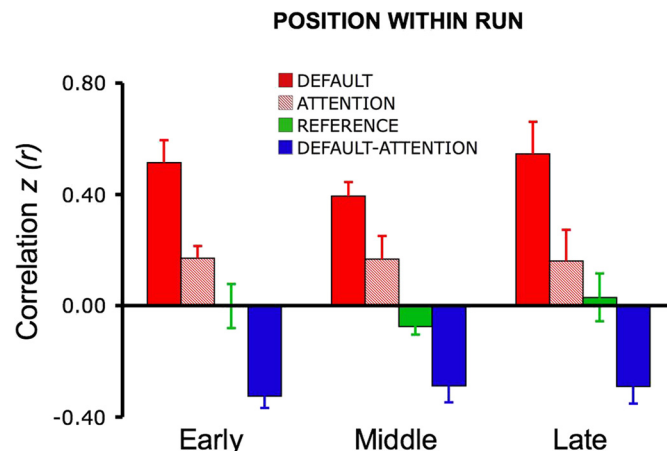

POSITION WITHIN RUN

FIG. 12. Functional connectivity strength is similar for early, middle, and late positions within a run. Functional connectivity strength within and between default, attention, and reference networks are depicted for rest data of 4 min each from the early, middle, and late periods of a 12-min run. Position within a run has minimal effect. Error bars represent SE.
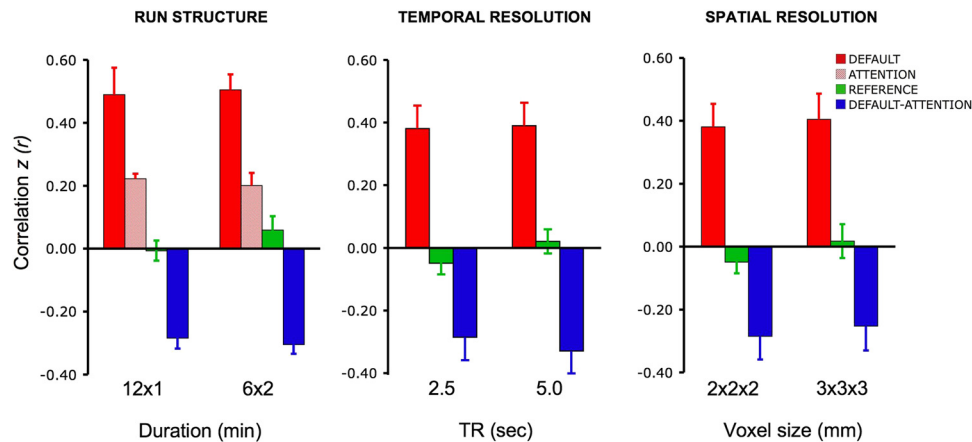
FIG. 13. Functional connectivity strength depends minimally on run structure, temporal resolution, and spatial resolution. Functional connectivity strengths are shown within and between default, attention, and reference networks for differences in the run structure (either 1 12-min run, or 2 6-min runs), temporal resolution (2.5 or 5.0 s TR), or spatial resolution (2 or 3 mm isotropic voxels). Comparisons between conditions did not reveal any statistically significant differences. Because higher temporal resolution required sampling only a portion of the brain (Dataset 3c), estimates of correlation strength among attention network regions were not available for temporal- and spatial resolution comparisons (see text).

ing the data-acquisition duration from one 5-min run to eight runs has only a marginal effect on reliability (Fig. 7). The upshot of these analyses is that studies involving only a single functional run are both feasible and efficient. Thus for situations where data loss is not expected, we suggest that for many purposes, a single fcMRI run is sufficient. There is one caveat to this recommendation. Noise decreased as a square root of the run length and statistical significance of correlations in individual subjects increased with increasing run length, indicating that longer duration acquisitions will yield more power for detecting smaller correlations and provide more precise estimates of the size of correlations. However, one can expect a substantial diminishing return with increasing run length or run numbers: a doubling of power will require a quadrupling of scan time.

BREAKS BETWEEN SCANS. Given that longer acquisition times may sometimes be desirable, we showed that two concatenated runs of 6 min provided virtually identical results when compared with a continuous run of 12 min. This result indicates that breaks between multiple, relatively short scans (e.g., 5 min) may be provided to participants, allowing greater feasibility for obtaining data in potentially difficult populations (e.g., children, older adults, patients). We did not find any benefit of using a continuous approach to data acquisition (see also Fair et al. 2007b for concatenation of even shorter duration epochs).

TASK DURING ACQUISITION. Our results indicate that a constant task (in this case, semantic classification) and resting with eyes closed result in less robust estimates of functional connectivity within the systems examined here. It remains possible that other systems will respond differently to other task settings. However, for applications requiring a robust estimate of the major large-scale brain systems identified to date, having participants simply rest with their eyes open is sufficient to acquire robust data without any additional equipment setup (see also C. Yan et al. 2009). Fully instructing participants on the importance of keeping their eyes open and monitoring compliance between scans are strongly recommended. Holding all factors equal, visual fixation is preferable because eye movements are better controlled; however, we could not detect a difference between eyes open with free viewing and fixation.

ROBUSTNESS TO REPETITION TIME AND SPATIAL RESOLUTION. We did not find substantial effects of varying temporal resolution between 2.5 and 5 s or spatial resolution between 2 and 3 mm. Researchers are therefore recommended to optimize these and other acquisition parameters for their scanner model and for study-specific purposes. In theory, poor temporal resolution will make it more difficult to appropriately estimate the low-frequency fluctuations that form the basis for fcMRI analysis and, in particular, removal of confounding signals (e.g., respiration). However, we could not detect a noticeable difference between 2.5- and 5.0-s repetition times. This is unlike event-
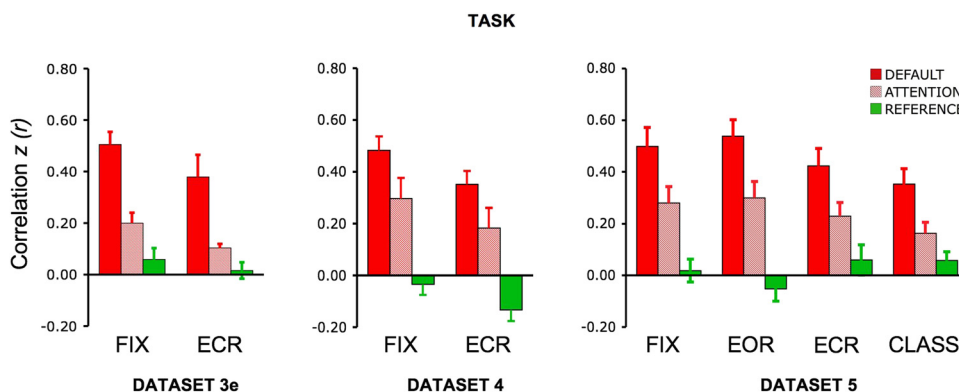

FIG. 14. Functional connectivity strength is influenced by task. Functional connectivity strengths are shown within default, attention, and reference networks while subject performed different tasks during data acquisition. Functional connectivity strength was significantly diminished for eyes closed rest (ECR) when compared with the fixation (fix) condition (see text). Having the subjects open their eyes (eyes open rest, EOR) mitigated this effect. Having the participants engage a continuous self-paced classification task (class) resulted in the weakest correlations. Thus having the subject rest with their eyes open or fixating generates the strongest correlations in the networks explored here. Error bars represent SE.

related fMRI procedures that are sensitive to repetition time changes in this time window (e.g., Miezin et al. 2000). There are two practical consequences of this observation. First, smaller voxel sizes can be used in whole-brain acquisition protocols to increase signal to noise (Triantafyllou et al. 2006) and reduce susceptibility artifacts. Smaller voxel sizes (e.g., 2 and 1 mm) are typically prohibitive for whole-brain imaging because of the necessarily long acquisition time to acquire each whole-brain volume. fcMRI is more robust to TR length than prior event-related fMRI techniques. Long TRs should therefore be considered as options (e.g., 3–5 s). Second, true whole-brain coverage including the full cerebellum can be readily obtained as many slices can be acquired with minimal loss of statistical power.

Relevance to human connectomics

As outlined in the INTRODUCTION, the field is entering a new era of exploration into human brain connectivity. The ultimate goal is to measure the complete connectional architecture of the human brain, referred to as the "connectome" (Sporns et al. 2005; see also Kasthuri and Lichtman 2007). A major reason for the surge in interest is the development of fcMRI and diffusion-based methods that hold promise for efficient and comprehensive analysis of the connectional architecture of the human brain.

There are three points to consider with regard to the potential role of fcMRI in these future efforts. First, fcMRI has strengths and limitations that are complementary to diffusion-based techniques. While fcMRI is highly sensitive, it is not specific to monosynaptic connections and is influenced by task states. This means fcMRI is primarily useful for identifying distinct connectivity patterns and differentiating large-scale circuits; it likely has limited utility for examining within-circuit details of connectivity and resolving monosynaptic connections. In contrast, diffusion-based methods that rely on HARDI techniques, such as DSI and Q-Ball methods, can contribute to resolving the details of anatomic connections but are unable to track pathways especially when they follow polysynaptic circuits through small structures such as the thalamus. In a detailed analysis of the statistical properties of fcMRI as contrasted with DSI tractography, Honey et al. (2009) concluded that fcMRI was more pervasive than structural connectivity, but that its spatial statistics are nonetheless constrained by the large-scale properties of anatomical connections. Based on these observations, fcMRI can be expected to be most useful as a tool to survey the broad topography of brain systems and global properties of brain architecture. Diffusion-based methods, in contrast, provide tools to more specifically unravel the details of anatomic projections.

Two recent papers that focus on cerebro-cerebellar circuitry provide a good illustration of the complementary strengths of fcMRI and diffusion-based methods. Granziera et al. (2009) used DSI to examine the detailed cerebellar pathways including the connections between the cerebellar cortex and the inferior olivary nucleus, the cerebellar cortex and the dentate nucleus, the deep cerebellar nuclei and the cerebellar peduncles, and the crossing intersections between the superior and inferior cerebellar peduncles. Each pathway was individually estimated by placing seeds in an initiating and target region. Many (but not all) of the expected cerebellar connec-

tions could be detected. The reconstructions were also able to visualize the tracts themselves including their complex 3D geometry. However, they were unable to follow the pathways across multiple synapses and map the full extent of the cerebro-cerebellar pathways themselves. That is, it was not possible to examine where a specific cerebellar region projects to in the cerebral cortex. If the networks were not known in advance, it would be difficult to determine their large-scale architecture from the DSI data alone. In contrast, Krienen and Buckner (2009), as discussed in the INTRODUCTION, applied fcMRI to estimate the distinct polysynaptic pathways that connect regions of the cerebellum to the neocortex (see also Habas et al. 2009; O'Reilly et al. 2009). Their fcMRI analysis was readily able to map and dissociate multiple projection zones of the cerebellum to the cerebral cortex (Fig. 15). However, the fcMRI analysis was unable to visualize the individuated stages of the pathways or resolve the details of the monosynaptic connections.

The analysis of Honey et al. (2009) and the contrasting discoveries made in the human cerebellum by DSI (Granziera et al. 2009) and fcMRI (Habas et al. 2009; Krienen and Buckner 2009; O'Reilly et al. 2009) illustrate that human connectomics will likely advance most rapidly by combining the complementary strengths of the two approaches. For this reason, it will be important to develop analytical methods and acquisition procedures that can align and maximize the mutual information provided by

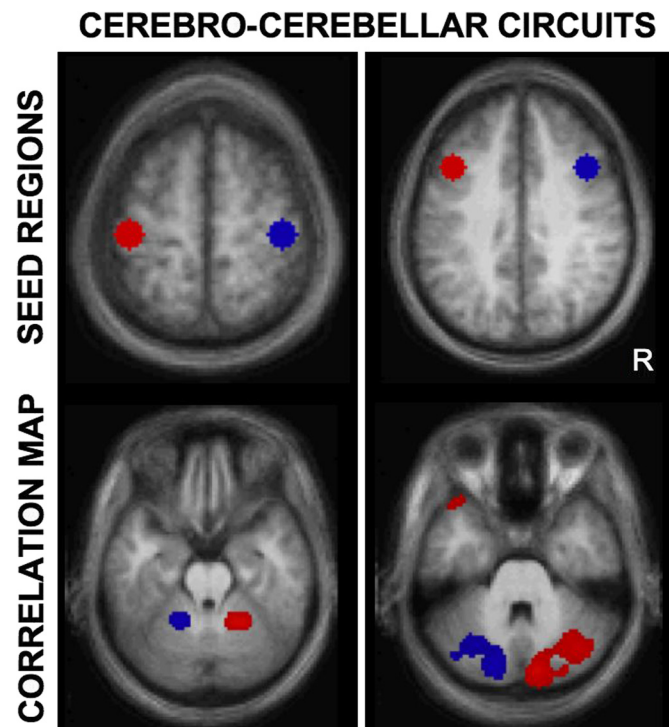## CEREBRO-CEREBELLAR CIRCUITS

FIG. 15. Functional connectivity reveals segregated fronto-cerebellar circuits. Two distinct cerebro-cerebellar circuits are mapped using right- and left seed regions (*top*) to illustrate the application of fcMRI and its sensitivity to detect anatomic circuitry. The cerebellar maps (*bottom*) display the functional connectivity differences between the lateralized seed regions. The maps reveal the contralateral projections of the cerebral cortex to the cerebellum and show segregated projections for motor (*left*) and prefrontal (*right*) circuits. The ability of fcMRI to map segregated, contralateral cerebellar projections from the cerebral cortex demonstrates that fcMRI is constrained by anatomy and also that functional correlations reflect polysynaptic connectivity. Adapted from Krienen and Buckner (2009).

diffusion-based and functional connectivity approaches (see Jbabdi et al. 2007 for relevant discussion).

The second point to consider about the role of fcMRI in human connectomics is that it will likely be limited. Neural circuits will ultimately be understood at the level of individual neuronal connections and the complex architecture of dendritic arbors. Mouse models have recently been developed that enable visualization of the details of local connectional architecture in small regions of the brain using genetically engineered fluorescence (Livet et al. 2007; see also Lichtman et al. 2008 for review). Electron microscopy approaches to serial reconstructions of neural tissue also show promise for tracking large numbers of individual axons (Briggman and Dank 2006; Hayworth et al. 2006).

Human fcMRI and diffusion-based methods will almost certainly be unable to approach the level of resolution required to track individual neuronal connections. For this reason, some have made a distinction between "connectomics" as the study of the individual neuronal connections and "projectomics" that examines the more global properties of areal projections (Kasthuri and Lichtman 2007). Within this distinction, fcMRI will likely play a role in elucidating the projectome but not in exploring the details of the connectome. A future direction will be to use animal models that are amenable to detailed analysis based on confocal and electron microscopy techniques as well as functional connectivity analysis via MRI to serve as bridges that can link the two levels of description. Also on the horizon is the possibility of using electron microscopic approaches on human tissue although significant advances will be required for sample and data handling.

The final point to consider about the use of fcMRI in connectomics arises from its efficiency. As the present studies demonstrate, acquisition times of as little as 5 or 6 min are sufficient to estimate global connectional properties of an individual person's brain. That is both surprising and remarkable. The efficiency of fcMRI may be a unique asset for the emerging field of brain genomics that seeks to understand the genetic determinants of brain structure and function. Until recently, structural MRI was the main source of information available about individual brain differences that could be linked to genetics, at least insofar as large sample sizes are required for genome-wide association studies and to explore interactions across multiple genetic variations. The efficiency of fcMRI, its reliability, and its robustness against small variations in acquisition parameters position it as a powerful tool for exploring genetic influences on brain architecture. We expect that datasets of thousands or even tens of thousands of subjects will become available over the next five years.

Conclusions

fcMRI detects correlations that are constrained by polysynaptic connectional anatomy and thus can be used to provide insight into the connectional architecture of the human brain. However, functional connectivity patterns are also affected by task states and fcMRI cannot resolve the direction of anatomic projections. fcMRI is particularly useful for characterizing large-scale brain systems that span distributed areas and has complementary strengths when contrasted with diffusion-based imaging techniques. Our empirical results suggest that, when common preprocessing procedures are applied, the measured correlation strengths

and the topography of correlation maps of well-known functional systems are reliable across subjects and sessions. Typical preprocessing procedures (including whole-brain signal regression) minimize physiological effects of respiration. In addition, fcMRI is minimally affected by differences in many acquisition parameters and can yield sufficient data for analysis in ~6 min. The brevity and robustness of the method positions fcMRI as a useful tool for large-scale normative studies and studies of individual variation, including those exploring genetic influences on brain architecture.

REFERENCES

Achard S, Salvador R, Whitcher B, Suckling J, Bullmore E. A resilient, low-frequency, small-world human brain functional network with highly connected association cortical hubs. *J Neurosci* 26: 63–72, 2006.

Aguirre GK, Zarahn E, D'Esposito M. Empirical analyses of BOLD fMRI statistics. II. Spatially smoothed data collected under null-hypothesis and experimental conditions. *Neuroimage* 5: 199–212, 1997.

Albert NB, Robertson EM, Miall RC. The resting human brain and motor learning. *Curr Biol* 19: 1023–1027, 2009.

Allen G, McColl R, Barnard H, Ringe WK, Fleckenstein J, Cullum CM. Magnetic resonance imaging of cerebellar-prefrontal and cerebellar-parietal functional connectivity. *Neuroimage* 28: 39–48, 2005.

Amann M, Hirsch JG, Gass A. A serial functional connectivity MRI study in healthy individuals assessing the variability of connectivity measures: Reduced interhemispheric connectivity in the motor network during continuous performance. *Magn Reson Imaging* 27: 1347–1359, 2009.

Anand A, Li Y, Wang Y, Lowe MJ, Dzemidzic M. Resting state corticolimbic connectivity abnormalities in unmedicated bipolar disorder and unipolar depression. *Psychiatry Res* 171: 189–198, 2009.

Anand A, Li Y, Wang Y, Wu J, Gao S, Bukhari L, Mathews VP, Kalnin A, Lowe MJ. Activity and connectivity of brain mood regulating circuit in depression: a functional magnetic resonance study. *Biol Psychiatry* 57: 1079–1088, 2005.

Andrews-Hanna JR, Snyder AZ, Vincent JL, Lustig C, Head D, Raichle ME, Buckner RL. Disruption of large-scale brain systems in advanced aging. *Neuron* 56: 924–935, 2007.

Antrobus JS. Information theory and stimulus-independent thought. *Br J Psychol* 59: 423–430, 1968.

Antrobus JS, Singer JL, Greenberg S. Studies in the stream of consciousness: experimental enhancement and suppression of spontaneous cognitive processes. *Percept Mot Skills* 23: 399–417, 1966.

Basser PJ, Pajevic S, Pierpaoli C, Duda J, Aldroubi A. In vivo fiber tractography using DT-MRI data. *Magn Reson Med* 44: 625–632, 2000.

Bassett DS, Bullmore E. Small-world brain networks. *Neuroscientist* 12: 512–523, 2006.

Bassett DS, Bullmore E. Human brain networks in health and disease. *Curr Opin Neurobiol* 22: 340–347, 2009.

Beckmann CF, DeLuca M, Devlin JT, Smith SM. Investigations into resting-state connectivity using independent component analysis. *Philos Trans R Soc Lond B Biol Sci* 360: 1001–1111, 2005.

Beckmann CF, Smith SM. Probabilistic independent component analysis for functional magnetic resonance imaging. *IEEE Trans Med Imaging* 23: 137–152, 2004.

Birn RM, Diamond JB, Smith MA, Bandettini PA. Separating respiratory-variation-related fluctuations from neuronal-activity-related fluctuations in fMRI. *Neuroimage* 31: 1536–1548, 2006.

Birn RM, Murphy K, Bandettini PA. The effect of respiration variations on independent component analysis results of resting state functional connectivity. *Hum Brain Mapp* 29: 740–750, 2008a.

Birn RM, Smith MA, Jones TB, Bandettini PA. The respiration response function: the temporal dynamics of fMRI signal fluctuations related to changes in respiration. *Neuroimage* 40: 644–654, 2008b.

Biswal B, Yetkin FZ, Haughton VM, Hyde JS. Functional connectivity in the motor cortex of resting human brain using echo-planar MRI. *Magn Reson Med* 34: 537–541, 1995.

Bluhm RL, Miller J, Lanius RA, Osuch EA, Boksman K, Neufeld RW, Theberge J, Schaefer B, Williamson P. Spontaneous low-frequency fluctuations in the BOLD signal in schizophrenic patients: anomalies in the default network. *Schizophr Bull* 33: 1004–1012, 2007.

Brainard DH. The psychophysics toolbox. *Spatial Vision* 10: 433–436, 1997.

Briggman KL, Denk W. Towards neural circuit reconstruction with volume electron microscopy techniques. *Curr Opin Neurobiol* 16: 562–570, 2006.

Buckner RL, Andrews-Hanna JR, Schacter DL. The brain's default network: anatomy, function, and relevance to disease. *Ann NY Acad Sci* 1124: 1–38, 2008.

Buckner RL, Sepulcre J, Talukdar T, Krienen FM, Liu H, Hedden T, Andrews-Hanna JR, Sperling RA, Johnson KA. Cortical hubs revealed by intrinsic functional connectivity: mapping, assessment of stability, and relation to Alzheimer's disease. *J Neurosci* 29: 1860–1873, 2009.

Buckner RL, Vincent JL. Unrest at rest: default activity and spontaneous network correlations. *Neuroimage* 37: 1091–1096, 2007.

Bullmore E, Sporns O. Complex brain networks: graph theoretical analysis of structural and functional systems. *Nat Rev Neurosci* 10: 186–198, 2009.

Burkhalter A, Bernardo KL, Charles V. Development of local circuits in human visual cortex. *J Neurosci* 13: 1916–1931, 1993.

Calhoun VD, Eichele T, Pearlson G. Functional brain networks in schizophrenia: a review. *Front Hum Neurosci* 3: 17, 2009.

Chang C, Cunningham JP, Glover GH. Influence of heart rate on the BOLD signal: the cardiac response function. *Neuroimage* 44: 857–869, 2009.

Chang C, Glover GH. Relationship between respiration, end-tidal CO2, and BOLD signals in resting-state fMRI. *Neuroimage* 47: 1381–1393, 2009a.

Chang C, Glover GH. Effects of model-based physiological noise correction on default mode network anti-correlations and correlations. *Neuroimage* 47: 1448–1459, 2009b.

Cherkassky VL, Kana RK, Keller TA, Just MA. Functional connectivity in a baseline resting-state network in autism. *Neuroreport* 17: 1687–1690, 2006.

Chuang KH, Chen JH. IMPACT: Image-based physiological artifacts estimation and correction technique for functional MRI. *Magn Reson Med* 46: 344–353, 2001.

Conturo TE, Lori NF, Cull TS, Akbudak E, Snyder AZ, Shimony J, McKinstry RS, Burton HS, Raichle ME. Tracking neuronal fiber pathways in the living human brain. *Proc Natl Acad Sci* 96: 10422–10427, 1999.

Corbetta M, Shulman GL. Control of goal-directed and stimulus-driven attention in the brain. *Nat Rev Neurosci* 3: 201–215, 2002.

Cordes D, Haughton VM, Arfanakis K, Wendt GJ, Turski PA, Moritz CH, Quigley MA, Meyerand ME. Mapping functionally related regions of brain with functional connectivity MR imaging. *Am J Neuroradiol* 21: 1636–1644, 2000.

Corfield DR, Murphy K, Josephs O, Adams L, Turner R. Does hypercapnia-induced cerebral vasodilation modulate the hemodynamic response to neural activation? *Neuroimage* 13: 1207–1211, 2001.

Dagli MS, Ingeholm JE, Haxby JV. Localization of cardiac-induced signal change in fMRI. *Neuroimage* 9: 407–415, 1999.

Damoiseaux JS, Beckmann CF, Arigita EJ, Barkhof F, Scheltens P, Stam CJ, Smith SM, Rombouts SA. Reduced resting-state brain activity in the "default network" in normal aging. *Cereb Cortex* 18: 1856–1864, 2008.

Damoiseaux JS, Greicius MD. Greater than the sum of its parts: a review of studies combining structural connectivity and resting-state functional connectivity. *Brain Struct Funct* 213: 525–533, 2009.

Damoiseaux JS, Rombouts SA, Barkhof F, Scheltens P, Stam CJ, Smith SM, Beckmann CF. Consistent resting-state networks across healthy subjects. *Proc Natl Acad Sci* 103: 13848–13853, 2006.

Deco G, Jirsa V, McIntosh AR, Sporns O, Kötter R. Key role of coupling, delay, and noise in resting brain fluctuations. *Proc Natl Acad Sci USA* 106: 10302–10307, 2009.

De Luca M, Beckmann CF, De Stefano N, Matthews PM, Smith SM. fMRI resting state networks define distinct modes of long-distance interactions in the human brain. *Neuroimage* 29: 1359–1367, 2006.

De Munck JC, Goncalves SI, Faes TJ, Kuijer JP, Pouwels PJ, Heethaar RM, Lopes da Silva FH. A study of the brain's resting state based on alpha band power, heart rate and fMRI. *Neuroimage* 42: 112–121, 2008.

Demb JB, Desmond JE, Wagner AD, Vaidya CJ, Glover GH, Gabrieli JD. Semantic encoding and retrieval in the left inferior prefrontal cortex: A functional MRI study of task difficulty and process specificity. *J Neurosci* 15: 5870–5878, 1995.

Desjardins AE, Kiehl KA, Liddle PF. Removal of confounding effects of global signal in functional MRI analyses. *Neuroimage* 13: 751–758, 2001.

D'Esposito M, Detre JA, Aguirre GK, Stallcup M, Alsop DC, Tippet LJ, Farah MJ. A functional MRI study of mental image generation. *Neuropsychologia* 35: 725–730, 1997.

Di Martino A, Scheres A, Margulies DS, Kelly AM, Uddin LQ, Shehzad Z, Biswal B, Walters JR, Castellanos FX, Milham MP. Functional connectivity of human striatum: a resting state FMRI study. *Cereb Cortex* 18: 2735–2747, 2008.

Evans AC, Collins DL, Mills SR, Brown ED, Kelly RL, Peters TM. 3D statistical neuroanatomical models from 305 MRI volumes. *Proc IEEE-Nuclear Scie Symp Med Imag Conf* 3: 1813–1817, 1993.

Evans KC, Dougherty DD, Schmid AM, Scannell E, McCallister A, Benson H, Dusek JA, Lazar SW. Modulation of spontaneous breathing via limbic/paralimbic-bulbar circuitry: an event-related fMRI study. *Neuroimage* 47: 961–971, 2009.

Fair DA, Cohen AL, Dosenbach NU, Church JA, Miezin FM, Barch DM, Raichle ME, Petersen SE, Schlaggar BL. The maturing architecture of the brain's default network. *Proc Natl Acad Sci* 105: 4028–4032, 2008.

Fair DA, Dosenbach NU, Church JA, Cohen AL, Brahmbhatt S, Miezin FM, Barch DM, Raichle ME, Petersen SE, Schlaggar BL. Development of distinct control networks through segregation and integration. *Proc Natl Acad Sci USA* 104: 13507–13512, 2007a.

Fair DA, Schlaggar BL, Cohen AL, Miezin FM, Dosenbach NU, Wenger KK, Fox MD, Snyder AZ, Raichle ME, Petersen SE. A method for using blocked and event-related fMRI data to study "resting state" functional connectivity. *Neuroimage* 35: 396–405, 2007b.

Fair DA, Cohen AL, Power JD, Dosenbach NU, Church JA, Miezin FM, Schlaggar BL, Petersen SE. Functional brain networks develop from a "local to distributed" organization. *PLoS Comput Biol* 5:e1000381, 2009.

Felleman DJ, Van Essen DC. Distributed hierarchical processing in the primate cerebral cortex. *Cereb Cortex* 1: 1–47, 1991.

Fox MD, Corbetta M, Snyder AZ, Vincent JL, Raichle ME. Spontaneous neuronal activity distinguishes human dorsal and ventral attention systems. *Proc Natl Acad Sci USA* 103: 10046–10051, 2006.

Fox MD, Raichle ME. Spontaneous fluctuations in brain activity observed with functional magnetic resonance imaging. *Nat Rev Neurosci* 8: 700–711, 2007.

Fox MD, Snyder AZ, Vincent JL, Corbetta M, Van Essen DC, Raichle ME. The human brain is intrinsically organized into dynamic, anticorrelated functional networks. *Proc Natl Acad Sci* 102: 9673–9678, 2005.

Fox MD, Zhang DY, Snyder AZ, Raichle ME. The global signal and observed anticorrelated resting state brain networks. *J Neurophysiol* 101: 3270–3283, 2009.

Fransson P. Spontaneous low-frequency BOLD signal fluctuations: an fMRI investigation of the resting-state default mode of brain function hypothesis. *Hum Brain Mapp* 26: 15–29, 2005.

Fransson P. How default is the default mode of brain function? Further evidence from intrinsic BOLD signal fluctuations. *Neuropsychologia* 44: 2836–2845, 2006.

Fransson P, Marrelec G. The precuneus/posterior cingulate cortex plays a pivotal role in the default mode network: evidence from a partial correlation network analysis. *Neuroimage* 42: 1178–1184, 2008.

Friston KJ. Functional and effective connectivity in neuroimaging: a synthesis. *Hum Brain Mapp* 2: 56–87, 1994.

Friston KJ, Frith CD, Liddle PF, Frackowiak RS. Functional connectivity: the principal-component analysis of large (PET) data sets. *J Cereb Blood Flow Metab* 13: 5–14, 1993.

Fukunaga M, Horovitz SG, van Gelderen P, de Zwart JA, Jansma JM, Ikonomidou VN, Chu RX, Deckers RH, Leopold DA, Duyn JH. Large-amplitude, spatially correlated fluctuations in BOLD fMRI signals during extended rest and early sleep stages. *Magn Reson Imaging* 24: 979–992, 2006.

Garrity AG, Pearlson GD, McKiernan K, Lloyd D, Kiehl KA, Calhoun VD. Aberrant "default mode" functional connectivity in schizophrenia. *Am J Psychiatry* 164: 450–457, 2007.

Geschwind N. Disconnexion syndromes in animals and man. Part 1. *Brain* 88: 237–294, 1965.

Ghosh A, Rho Y, McIntosh AR, Kötter R, Jirsa VK. Noise during rest enables the exploration of the brain's dynamic repertoire. *PLoS Comput Biol* 4: e1000196, 2008.

Glover GH, Li TQ, Ress D. Image-based method for retrospective correction of physiological motion effects in fMRI: RETROICOR. *Magn Reson Med* 44: 162–167, 2000.

Gochin PM, Miller EK, Gross CG, Gerstein GL. Functional interactions among neurons in inferior temporal cortex of the awake macaque. *Exp Brain Res* 84: 505–516, 1991.

Granziera C, Schmahmann JD, Hadjikhani N, Meyer H, Meuli R, Wedeen V, Krueger G. Diffusion spectrum imaging shows the structural basis of functional cerebellar circuits in the human cerebellum in vivo. *PLoS One* 4: e5101, 2009.

Greicius M. Resting-state functional connectivity in neuropsychiatric disorders. *Curr Opin Neurol* 21: 424–430, 2008.

Greicius MD, Flores BH, Menon V, Glover GH, Solvason HB, Kenna H, Reiss AL, Schatzberg AF. Resting-state functional connectivity in major depression: abnormally increased contributions from subgenual cingulate cortex and thalamus. *Biol Psychiatry* 62: 429–437, 2007.

Greicius MD, Kiviniemi V, Tervonen O, Vainionpää V, Alahuhta S, Reiss AL, Menon V. Persistent default-mode network connectivity during light sedation. *Hum Brain Mapp* 29: 839–847, 2008.

Greicius MD, Krasnow B, Reiss AL, Menon V. Functional connectivity in the resting brain: a network analysis of the default mode hypothesis. *Proc Natl Acad Sci* 100: 253–258, 2003.

Greicius MD, Srivastava G, Reiss AL, Menon V. Default-mode network activity distinguishes Alzheimer's disease from healthy aging: evidence from functional MRI. *Proc Natl Acad Sci* 101: 4637–4642, 2004.

Greicius MD, Supekar K, Menon V, Dougherty RF. Resting-state functional connectivity reflects structural connectivity in the default mode network. *Cereb Cortex* 19: 72–78, 2009.

Habas C, Kamdar N, Nguyen D, Prater K, Beckmann CF, Menon V, Greicius MD. Distinct cerebellar contributions to intrinsic connectivity networks. *J Neurosci* 29: 8586–8594, 2009.

Hagmann P, Cammoun L, Gigandet X, Meuli R, Honey CJ, Wedeen VJ, Sporns O. Mapping the structural core of human cerebral cortex. *PLoS Biol* 6: e159, 2008.

Hampson M, Peterson BS, Skudlarski P, Gatenby JC, Gore JC. Detection of functional connectivity using temporal correlations in MR images. *Hum Brain Mapp* 15: 247–262, 2002.

Hampson M, Olson IR, Leung HC, Skudlarski P, Gore JC. Changes in functional connectivity of human MT/V5 with visual motion input. *Neuroreport* 15: 1315–1319, 2004.

Hasson U, Nusbaum HC, Small SL. Task-dependent organization of brain regions active during rest. *Proc Natl Acad Sci* 106: 10841–10846, 2009.

Haughton V, Biswal B. Clinical application of basal regional cerebral blood flow fluctuation measurements by fMRI. *Adv Exp Med Biol* 454: 583–590, 1998.

Hayworth KJ, Kasthuri N, Schalek R, Lichtman JW. Automating the collection of ultrathin serial sections for large volume TEM reconstructions. *Microsc Microanal* 12, Supplement 2: 86–87, 2006.

Hedden T, Van Dijk KRA, Becker JA, Mehta A, Sperling RA, Johnson KA, Buckner RL. Disruption of functional connectivity in clinically normal older adults harboring amyloid burden. *J Neurosci* 29: 12686–12694, 2009.

Honey CJ, Kötter R, Breakspear M, Sporns O. Network structure of cerebral cortex shapes functional connectivity on multiple time scales. *Proc Natl Acad Sci* 104: 10240–10245, 2007.

Honey CJ, Sporns O, Cammoun L, Gigandet X, Thiran JP, Meuli R, Hagmann P. Predicting human resting-state functional connectivity from structural connectivity. *Proc Natl Acad Sci* 106: 2035–2040, 2009.

Horovitz SG, Fukunaga M, de Zwart JA, van Gelderen P, Fulton SC, Balkin TJ, Duyn JH. Low frequency BOLD fluctuations during resting wakefulness and light sleep: a simultaneous EEG-fMRI study. *Hum Brain Mapp* 29: 671–682, 2008.

Horovitz SG, Braun AR, Carr WS, Picchioni D, Balkin TJ, Fukunaga M, Duyn JH. Decoupling of the brain's default mode network during deep sleep. *Proc Natl Acad Sci USA* 106: 11376–11381, 2009.

Horwitz B. The elusive concept of brain connectivity. *Neuroimage* 19: 466–470, 2003.

Horwitz B, Duara R, Rapoport SI. Intercorrelations of glucose metabolic rates between brain regions: application to healthy males in a state of reduced sensory input. *J Cereb Blood Flow Metab* 4: 484–499, 1984.

Hunter MD, Eickhoff SB, Miller TW, Farrow TF, Wilkinson ID, Woodruff PW. Neural activity in speech-sensitive auditory cortex during silence. *Proc Natl Acad Sci* 103: 189–194, 2006.

Jbabdi S, Woolrich MW, Andersson JLR, Behrens TEJ. A Bayesian framework for global topography. *Neuroimage* 37: 116–129, 2007.

Jenkins GM, Watts DG. *Spectral Analysis and its Applications.* Boca Raton, FL: Emerson–Adams, 1968.

Jenkinson M, Bannister P, Brady M, Smith S. Improved optimization for the robust and accurate linear registration and motion correction of brain images. *Neuroimage* 17: 825–841, 2002.

Johnston JM, Vaishnavi SN, Smyth MD, Zhang DY, He BJ, Zempel JM, Shimony JS, Snyder AZ, Raichle ME. Loss of resting interhemispheric functional connectivity after complete section of the corpus callosum. *J Neurosci* 28: 6453–6458, 2008.

Jones EG, Powell TP. An anatomical study of converging sensory pathways within the cerebral cortex of the monkey. *Brain* 93: 793–820, 1970.

Kahn I, Andrews-Hanna JR, Vincent JL, Snyder AZ, Buckner RL. Distinct cortical anatomy linked to subregions of the medial temporal lobe revealed by intrinsic functional connectivity. *J Neurophysiol* 100: 129–139, 2008.

Kasthuri N, Lichtman JW. The rise of the "projectome." *Nat Methods* 4: 307–308, 2007.

Kelly AM, Uddin LQ, Biswal BB, Castellanos FX, Milham MP. Competition between functional brain networks mediates behavioral variability. *Neuroimage* 39: 527–537, 2008.

Kelly AM, Di Martino A, Uddin LQ, Shehzad Z, Gee DG, Reiss PT, Margulies DS, Castellanos FX, Milham MP. Development of anterior cingulate functional connectivity from late childhood to early adulthood. *Cereb Cortex* 19: 640–657, 2009.

Kelly RM, Strick PL. Cerebellar loops with motor cortex and prefrontal cortex of a nonhuman primate. *J Neurosci* 23: 8432–8444, 2003.

Kennedy DP, Courchesne E. The intrinsic functional organization of the brain is altered in autism. *Neuroimage* 3: 1877–1885, 2008.

Koch MA, Norris DG, Hund-Georgiadis M. An investigation of functional and anatomical connectivity using magnetic resonance imaging. *Neuroimage* 16: 241–250, 2002.

Kondakor I, Brandeis D, Wackermann J, Kochi K, Koenig T, Frei E, Pascual-Marqui RD, Yagyu T, Lehmann D. Multichannel EEG fields during and without visual input: frequency domain model source locations and dimensional complexities. *Neurosci Lett* 226: 49–52, 1997.

Krienen FM, Buckner RL. Segregated fronto-cerebellar circuits revealed by intrinsic functional connectivity. *Cereb Cortex* 19: 2485–2497, 2009.

Kwong KK, Belliveau JW, Chesler DA, Goldberg IE, Weisskoff RM, Poncelet BP, Kennedy DN, Hoppel BE, Cohen MS, Turner R, Cheng HM, Brady TJ, Rosen BR. Dynamic magnetic resonance imaging of human brain activity during primary sensory stimulation. *Proc Natl Acad Sci* 89: 5675–5679, 1992.

Larson-Prior LJ, Zempel JM, Nolan TS, Prior FW, Snyder AZ, Raichle ME. Cortical network functional connectivity in the descent to sleep. *Proc Natl Acad Sci* 106: 4489–494, 2009.

Le Bihan D, Mangin JF, Poupon C, Clark CA, Pappata S, Molko N, Chabriat H. Diffusion tensor imaging: concepts and applications. *J Magn Reson Imaging* 13: 534–546, 2001.

Lewis CM, Baldassarre A, Committeri G, Luca Romani G, Corbetta M. Learning sculpts the spontaneous activity of the resting human brain. *Proc Natl Acad Sci* 106: 17558–17563, 2009.

Lewis JW, Van Essen DC. Mapping of architectonic subdivisions in the macaque monkey, with emphasis on parieto-occipital cortex. *J Comp Neurol* 428: 79–111, 2000.

Lichtman JW, Livet J, Sanes JR. A technicolor approach to the connectome. *Nat Rev Neurosci* 9: 417–422, 2008.

Liu H, Buckner RL, Talukdar T, Tanaka N, Madsen JR, Stufflebeam SM. Task-free presurgical mapping using functional magnetic resonance imaging intrinsic activity. *J Neurosurg* 111: 746–754, 2009a.

Liu H, Stufflebeam SM, Sepulcre J, Hedden T, Buckner RL. Evidence that functional asymmetry of the human brain is controlled by multiple factors. *Proc Natl Acad Sci* 111: 746–754, 2009b.

Livet J, Weissman TA, Kang H, Draft RW, Lu J, Bennis RA, Sanes JR, Lichtman JW. Transgenic strategies for combinatorial expression of fluorescent proteins in the nervous system. *Nature* 450: 56–62, 2007.

Long XY, Zuo XN, Kiviniemi V, Yang Y, Zou QH, Zhu CZ, Jiang TZ, Yang H, Gong QY, Wang L, Li KC, Xie S, Zang YF. Default mode network as revealed with multiple methods for resting-state functional MRI analysis. *J Neurosci Methods* 171: 349–355, 2008.

Lowe MJ, Mock BJ, Sorenson JA. Functional connectivity in single and multislice echoplanar imaging using resting-state fluctuations. *Neuroimage* 7: 119–132, 1998.

Lund TE, Madsen KH, Sidaros K, Luo WL, Nichols TE. Non-white noise in fMRI: Does modelling have an impact? *Neuroimage* 29: 54–66, 2006.

Macey PM, Macey KE, Kumar R, Harper RM. A method for removal of global effects from fMRI time series. *Neuroimage* 22: 360–366, 2004.

Margulies DS, Kelly AM, Uddin LQ, Biswal BB, Castellanos FX, Milham MP. Mapping the functional connectivity of anterior cingulate cortex. *Neuroimage* 37: 579–588, 2007.

Margulies DS, Vincent JL, Kelly C, Lohmann G, Uddin LQ, Biswal BB, Villringer A, Castellanos FX, Milham MP, Petrides M. Precuneus shares intrinsic functional architecture in humans and monkeys. *Proc Natl Acad Sci* doi:10.1073/pnas.0905314106.

McIntosh AR. Mapping cognition to the brain through neural interactions. *Memory* 7: 523–548, 1999.

Meindl T, Teipel S, Elmouden R, Mueller S, Koch W, Dietrich O, Coates U, Reiser M, Glaser C. Test-retest reproducibility of the default-mode network in healthy individuals. *Hum Brain Mapp* doi:10.1016/j.neuroimage.2009.10.067.

Mesulam M-M. From sensation to cognition. *Brain* 121: 1013–1052, 1998.

Mesulam M-M. *Principles of Behavioral and Cognitive Neurology.* New York: Oxford Univ. Press, 2000.

Meunier D, Achard S, Morcom A, Bullmore E. Age-related changes in modular organization of human brain functional networks. *Neuroimage* 44: 715–723, 2009.

Middleton FA, Strick PL. Basal ganglia output and cognition: evidence from anatomical, behavioral, and clinical studies. *Brain Cogn* 42: 183–200, 2000.

Miezin FM, Maccotta L, Ollinger JM, Petersen SE, Buckner RL. Characterizing the hemodynamic response: effects of presentation rate, sampling procedure, and the possibility of ordering brain activity based on relative timing. *Neuroimage* 11: 735–759, 2000.

Minka T. *Automatic Choice of Dimensionality for PCA.* MIT Media Lab Vision and Modeling Group, 2000 (Technical Report 514).

Mori S, Kaufmann WE, Davatzikos C, Stieltjes B, Amodei L, Fredericksen K, Pearlson GD, Melhem ER, Solaiyappan M, Raymond GV, Moser HW, van Ziji PC. Imaging cortical association tracts in the human brain using diffusion-tensor-based axonal tracking. *Magn Reson Med* 47: 215–223, 2002.

Murphy K, Birn RM, Handwerker DA, Jones TB, Bandettini PA. The impact of global signal regression on resting state correlations: are anti-correlated networks introduced? *Neuroimage* 44: 893–905, 2009.

Newton AT, Morgan VL, Gore JC. Task demand modulation of steady-state functional connectivity to primary motor cortex. *Hum Brain Mapp* 28: 663–672, 2007.

Nunez PL, Srinivasan R, Westdorp AF, Wijesinghe RS, Tucker DM, Silberstein RB, Cadusch PJ. EEG coherency. I. Statistics, reference electrode, volume conduction, Laplacians, cortical imaging, and interpretation at multiple scales. *Electroencephalogr Clin Neurophysiol* 103: 499–515, 1997.

Ogawa S, Tank DW, Menon RS, Ellermann JM, Kim SG, Merkle H, Ugurbil K. Intrinsic signal changes accompanying sensory stimulation: functional brain mapping with magnetic resonance imaging. *Proc Natl Acad Sci* 89: 5951–5955, 1992.

O'Reilly JX, Beckmann CF, Tomassini V, Ramnani N, Johansen-Berg H. Distinct and overlapping functional zones in the cerebellum defined by resting state functional connectivity. *Cereb Cortex* doi:10.1093/cercor/bhp157.

Pandya DN, Kuypers HG. Cortico-cortical connections in the rhesus monkey. *Brain Res* 13: 13–36, 1969.

Pascual-Leone A, Walsh V, Rothwell J. Transcranial magnetic stimulation in cognitive neuroscience—virtual lesion, chronometry, and functional connectivity. *Curr Opin Neurobiol* 10: 232–237, 2000.

Paus T, Jech R, Thompson CJ, Comeau R, Peters T, Evans AC. Transcranial magnetic stimulation during positron emission tomography: a new method for studying connectivity of the human cerebral cortex. *J Neurosci* 17: 3178–3184, 1997.

Popa D, Popescu AT, Paré D. Contrasting activity profile of two distributed cortical networks as a function of attentional demands. *J Neurosci* 29: 1191–1201, 2009.

Raichle ME, MacLeod AM, Snyder AZ, Powers WJ, Gusnard DA, Shulman GL. A default mode of brain function. *Proc Natl Acad Sci* 98: 676–682, 2001.

Roy AK, Shehzad Z, Margulies DS, Kelly AM, Uddin LQ, Gotimer K, Biswal BB, Castellanos FX, Milham MP. Functional connectivity of the human amygdala using resting state fMRI. *Neuroimage* 45: 614–626, 2009.

Rubinov M, Sporns O. Complex network measures of brain connectivity: uses and interpretations. *Neuroimage* doi:10.1016/j.neuroimage.2009.10.003.

Schmahmann JD, Doyon J, McDonald D, Holmes C, Lavoie K, Hurwitz AS, Kabani N, Toga A, Evans A, Petrides M. Three-dimensional MRI atlas of the human cerebellum in proportional stereotaxic space. *Neuroimage* 10: 233–260, 1999.

Schmahmann JD, Doyon J, Toga A, Evans A, Petrides M. *MRI Atlas of the Human Cerebellum.* San Diego, CA: Academic, 2000.

Schmahmann JD, Weilburg JB, Sherman JC. The neuropsychiatry of the cerebellum—insights from the clinic. *Cerebellum* 6: 254–267, 2007.

Seeley WW, Crawford RK, Zhou J, Miller BL, Greicius MD. Neurodegenerative diseases target large-scale human brain networks. *Neuron* 62: 42–52, 2009.

Shehzad Z, Kelly AM, Reiss PT, Gee DG, Gotimer K, Uddin LQ, Lee SH, Margulies DS, Roy AK, Biswal BB, Petkova E, Castellanos FX, Milham MP. The resting brain: unconstrained yet reliable. *Cereb Cortex* 19: 2209–2229, 2009.

Sheline YI, Raichle ME, Snyder AZ, Morris JC, Head D, Wang S, Mintun MA. Amyloid plaques disrupt resting state default mode network connectivity in cognitively normal elderly. *Biol Psychiatry* In press.

Sherbondy AJ, Dougherty RF, Ben-Shachar M, Napel S, Wandell BA. ConTrack: finding the most likely pathways between brain regions using diffusion tractography. *J Vis* 8: 1–16, 2008.

Shimony JS, Zhang D, Johnston JM, Fox MD, Roy A, Leuthardt EC. Resting-state spontaneous fluctuations in brain activity: a new paradigm for presurgical planning using fMRI. *Acad Radiol* 16: 578–583, 2009.

Shmueli K, van Gelderen P, de Zwart JA, Horovitz SG, Fukunaga M, Jansma JM, Duyn JH. Low-frequency fluctuations in the cardiac rate as a source of variance in the resting-state fMRI BOLD signal. *Neuroimage* 38: 306–320, 2007.

Smith SM, Fox PT, Miller KL, Glahn DC, Mickle Fox P, Mackay CE, Filippini N, Watkins KE, Toro R, Laird AR, Beckmann CF. Correspondence of the brain's functional architecture during activation and rest. *Proc Natl Acad Sci* 106: 13040–13045, 2009.

Sorg C, Riedl V, Mühlau M, Calhoun VD, Eichele T, Läer L, Drzezga A, Förstl H, Kurz A, Zimmer C, Wohlschläger AM. Selective changes of resting-state networks in individuals at risk for Alzheimer's disease. *Proc Natl Acad Sci* 104: 18760–18765, 2007.

Sporns O, Honey CJ, Kötter R. Identification and classification of hubs in brain networks. *PLoS One* 2: e1049, 2007.

Sporns O, Tononi G, Kötter R. The human connectome: a structural description of the human brain. *PLoS Comput Biol* 1: e42, 2005.

Triantafyllou C, Hoge RD, Wald LL. Effect of spatial smoothing on physiological noise in high-resolution fMRI. *Neuroimage* 32: 551–557, 2006.

Tuch DS, Reese TG, Wiegell MR, Makris N, Belliveau JW, Wedeen VJ. High angular resolution diffusion imaging reveals intravoxel white matter fiber heterogeneity. *Magn Reson Med* 48: 577–582, 2002.

Uddin LQ, Kelly AM, Biswal BB, Margulies DS, Shehzad Z, Shaw D, Ghaffari M, Rotrosen J, Adler LA, Castellanos FX, Milham MP. Network homogeneity reveals decreased integrity of default-mode network in ADHD. *J Neurosci Methods* 169: 249–254, 2008.

Uddin LQ, Kelly AM, Biswal BB, Xavier Castellanos F, Milham MP. Functional connectivity of default mode network components: correlation, anticorrelation, and causality. *Hum Brain Mapp* 30: 625–637, 2009.

Ungerleider LG, Haxby JV. "What" and "where" in the human brain. *Curr Opin Neurobiol* 4: 157–165, 1994.

Van Buuren M, Gladwin TE, Zandbelt BB, van den Heuvel M, Ramsey NF, Kahn RS, Vink M. Cardiorespiratory effects on default-mode network activity as measured with fMRI. *Hum Brain Mapp* 30: 3031–3042, 2009.

Van de Ven VG, Formisano E, Prvulovic D, Roeder CH, Linden DE. Functional connectivity as revealed by spatial independent component analysis of fMRI measurements during rest. *Hum Brain Mapp* 22: 165–178, 2004.

Vincent JL, Kahn I, Snyder AZ, Raichle ME, Buckner RL. Evidence for a frontoparietal control system revealed by intrinsic functional connectivity. *J Neurophysiol* 100: 3328–3342, 2008.

Vincent JL, Patel GH, Fox MD, Snyder AZ, Baker JT, Van Essen DC, Zempel JM, Snyder LH, Corbetta M, Raichle ME. Intrinsic functional architecture in the anesthetized monkey brain. *Nature* 447: 83–86, 2007.

Vincent JL, Snyder AZ, Fox MD, Shannon BJ, Andrews JR, Raichle ME, Buckner RL. Coherent spontaneous activity identifies a hippocampal-parietal memory network. *J Neurophysiol* 96: 3517–3531, 2006.

Vogt BA, Vogt L, Laureys S. Cytology and functionally correlated circuits of human posterior cingulate areas. *Neuroimage* 29: 452–466, 2006.

Wagner AD, Schacter DL, Rotte M, Koutstaal W, Maril A, Dale AM, Rosen BR, Buckner RL. Building memories: remembering and forgetting of verbal experiences as predicted by brain activity. *Science* 281: 1188–1191, 1998.

Wang K, Liang M, Wang L, Tian L, Zhang X, Li K, Jiang T. Altered functional connectivity in early Alzheimer's disease: a resting-state fMRI study. *Hum Brain Mapp* 28: 967–978, 2007.

Waites AB, Stanislavsky A, Abbott DF, Jackson GD. Effect of prior cognitive state on resting state networks measured with functional connectivity. *Hum Brain Mapp* 24: 59–68, 2005.

Watts DJ, Strogatz SH. Collective dynamics of "small-world" networks. *Nature* 393: 440–442, 1998.

Wedeen VJ, Hagmann P, Tseng WY, Reese TG, Weisskoff RM. Mapping complex tissue architecture with diffusion spectrum magnetic resonance imaging. *Magn Reson Med* 54: 1377–1386, 2005.

Weissenbacher A, Kasess C, Gerstl F, Lanzenberger R, Moser E, Windischberger C. Correlations and anticorrelations in resting-state functional connectivity MRI: a quantitative comparison of preprocessing strategies. *Neuroimage* 47: 1408–1416, 2009.

Whitfield-Gabrieli S, Thermenos HW, Milanovic S, Tsuang MT, Faraone SV, McCarley RW, Shenton ME, Green AI, Nieto-Castanon A, LaViolette P, Wojcik J, Gabrieli JD, Seidman LJ. Hyperactivity and hyperconnectivity of the default network in schizophrenia and in first-degree relatives of persons with schizophrenia. *Proc Natl Acad Sci* 106: 1279–1284, 2009.

Windischberger C, Langenberger H, Sycha T, Tschernko EM, Fuchsjager-Mayerl G, Schmetterer L, Moser E. On the origin of respiratory artifacts in BOLD-EPI of the human brain. *Magn Reson Imaging* 20: 575–582, 2002.

Wise RG, Ide K, Poulin MJ, Tracey I. Resting fluctuations in arterial carbon dioxide induce significant low frequency variations in BOLD signal. *Neuroimage* 21: 1652–1664, 2004.

Wu CW, Gu H, Lu H, Stein EA, Chen JH, Yang Y. Frequency specificity of functional connectivity in brain networks. *Neuroimage* 42: 1047–1055, 2008.

Yan L, Wu Y, Wu D, Qin S, Xu G. Pattern analysis of motor functional connectivity. *Funct Neurol* 23: 141–147, 2008.

Yan H, Zuo XN, Wang D, Wang J, Zhu C, Milham MP, Zhang D, Zang Y. Hemispheric asymmetry in cognitive division of anterior cingulate cortex: a resting-state functional connectivity study. *Neuroimage* 47: 1579–1589, 2009.

Yan C, Liu D, He Y, Zou Q, Zhu C, Zuo X, Long X, Zang Y. Spontaneous brain activity in the default mode network is sensitive to different resting-state conditions with limited cognitive load. *PLoS One* 4: e5743, 2009.

Yang H, Long XY, Yang Y, Yan H, Zhu CZ, Zhou XP, Zang YF, Gong QY. Amplitude of low frequency fluctuation within visual areas revealed by resting-state functional MRI. *Neuroimage* 36: 144–152, 2007.

Zar JH. *Biostatistical Analysis.* Upper Saddle River NJ: Prentice Hall, 1996.

Zhang D, Snyder AZ, Fox MD, Sansbury MW, Shimony JS, Raichle ME. Intrinsic functional relations between human cerebral cortex and thalamus. *J Neurophysiol* 100: 1740–1748, 2008.

Zhou Y, Dougherty JH, Jr, Hubner KF, Bai B, Cannon RL, Hutson RK. Abnormal connectivity in the posterior cingulate and hippocampus in early Alzheimer's disease and mild cognitive impairment. *Alzheimers Dement* 4: 265–270, 2008.

Zhou Y, Liang M, Tian L, Wang K, Hao Y, Liu H, Liu Z, Jiang T. Functional disintegration in paranoid schizophrenia using resting-state fMRI. *Schizophr Res* 97: 194–205, 2007.

Zuo XN, Di Martino A, Kelly C, Shehzad ZE, Gee DG, Klein DF, Castellanos FX, Biswal BB, Milham MP. The oscillating brain: complex and reliable. *Neuroimage* 2009 doi:10.1016/j.neuroimage.2009.09.037.